Polyamorphism and liquid–liquid phase transitions: challenges for experiment and theory

2007 J. Phys.: Condens. Matter 19 415101

(http://iopscience.iop.org/0953-8984/19/41/415101)

IOP PUBLISHING JOURNAL OF PHYSICS: CONDENSED MATTER

J. Phys.: Condens. Matter **19** (2007) 415101 (41pp) doi:10.1088/0953-8984/19/41/415101

Polyamorphism and liquid–liquid phase transitions: challenges for experiment and theory*

Paul F McMillan[1,2,5], Mark Wilson[1], Martin C Wilding[3], Dominik Daisenberger[1], Mohamed Mezouar[4] and G Neville Greaves[3]

[1] Department of Chemistry and Materials Chemistry Centre, University College London, 20 Gordon Street, London WC1H 0AJ, UK
[2] Davy-Faraday Research Laboratory, Royal Institution of Great Britain, 21 Albemarle Street, London W1X 4BS, UK
[3] Institute of Mathematics and Physical Sciences, University of Wales at Aberystwyth, Ceredigion SY23 3BZ, UK
[4] European Synchrotron Radiation Facility, BP 220, F-38043, Grenoble, France

E-mail: p.f.mcmillan@ucl.ac.uk

Received 31 May 2007, in final form 2 July 2007
Published 27 September 2007
Online at stacks.iop.org/JPhysCM/19/415101

Abstract

Phase transitions in the liquid state can be related to pressure-driven fluctuations developed in the density (i.e., the inverse of the molar volume; $\rho = 1/V$) or the entropy ($S(T)$) rather than by gradients in the chemical potential ($\mu(X)$, where X is the chemical composition). Experiments and liquid simulation studies now show that such transitions are likely to exist within systems with a wide range of chemical bonding types. The observations permit us to complete the trilogy of expected liquid state responses to changes in P and T as well as $\mu(X)$, as is the case among crystalline solids. Large structure–property changes occurring within non-ergodic amorphous solids as a function of P and T are also observed, that are generally termed 'polyamorphism'. The polyamorphic changes can map on to underlying density- or entropy-driven L–L transitions. Studying these phenomena poses challenges to experimental studies and liquid simulations. Experiments must be carried out over a wide P–T range for *in situ* structure–property determinations, often in a highly metastable regime. It is expected that L–L transitions often occur below the melting line, so that studies encounter competing crystallization phenomena. Simulation studies of liquid state polyamorphism must involve large system sizes, and examine system behaviour at low T into the deeply supercooled regime, with distance and timescales long enough to sample characteristic density/entropy fluctuations. These conditions must be achieved for systems with different bonding environments, that can change abruptly across the polyamorphic

* This paper is presented as a contribution to the conference on 'Current Challenges in Liquid and Glass Science' held in Abingdon, UK, January 10–12, 2007 in honour of Spencer Howells.

[5] Author to whom any correspondence should be addressed.

transitions. Here we discuss opportunities for future work using simulations combined with neutron and x-ray amorphous scattering techniques, with special reference to the behaviour of two polyamorphic systems: amorphous Si and supercooled Y_2O_3–Al_2O_3 liquids.

1. Introduction

1.1. Melting curve maxima, the two-state model, and the likely occurrence of density-, entropy-driven liquid–liquid phase transitions

The occurrence of liquid–liquid phase transitions driven by gradients in the chemical potential (i.e. $\mu(X)$, where X is a compositional variable) leads to the well known phenomenon of 'unmixing', that occurs between liquids with different chemical compositions and also among corresponding amorphous solids below their glass transformation range. Among crystalline solids, however, density- or entropy-driven phase transitions between polymorphs with identical chemical composition are also well known to occur as a function of the pressure (P) and temperature (T). The possibility that analogous transformations might occur within the liquid state has not yet been fully developed, partly because it is known that liquids possess a time-averaged dynamic structure, and it has generally been thought that changes in structure and thermodynamic properties in response to P and T variables should occur continuously rather than correspond to an abrupt phase transition. An obvious exception to this premise already occurs in the behaviour of liquid crystals, for which thermodynamically well defined phases occur in distinct P–T regions as a function of the relative orientation and packing of polymer species. Another exception occurs in the case of liquid helium, in which quantum fluctuations determine thermodynamic transitions between distinct liquid phases. However, the existence of three-dimensional L–L phase transitions within classical isotropic systems at constant chemical composition, involving density or entropy differences between the different liquid phases, is only just beginning to be investigated and understood [1–9]. Development of this new field of research into the fundamental physical chemistry of liquids and amorphous solids poses challenges for both theoretical and experimental studies, including neutron and x-ray scattering science, that are highlighted in this paper.

The prediction that liquid–liquid phase transitions should occur at constant chemical composition in response to changes in the density first arose from the analysis of unusual melting relations that were observed for various elements and simple compounds at high P. Generally, the entropy of a system must increase upon melting; i.e., $\Delta S_m > 0$. The corresponding volume change is also usually expected to be positive ($\Delta V_m > 0$), so that the melting relation (dT_m/dP) has a positive slope, according to the Clausius–Clapeyron relation:

$$\frac{dT_m}{dP} = \frac{\Delta V_m}{\Delta S_m}. \tag{1}$$

Experimental determinations of dT_m/dP have been carried out for many elements and compounds, beginning with the pioneering work of Bridgman and other high-pressure researchers [10, 11]. Studies in the field continue to the present day, and they have major implications for planetary sciences and materials research, although there still exist disagreements between various works even for some of the most apparently 'simple' systems [12–16]. Although T_m measured for most systems is found to increase with P as predicted, some elements and compounds studied in the early experiments (H_2O, Ga, Bi, H_2O and Si, Ge, Ti, Pu, α-GeO_2 and Li_2MoO_4 determined in later studies) were observed to have unusual *negative* initial melting slopes. For H_2O (ice Ih) that phenomenon was expected to

occur from the classical observation that the liquid is more dense than the crystalline solid (i.e., ice floats on water), that could be generally explained by H-bonding differences occurring within the liquid versus the crystalline state. However, the density increase upon melting observed within other systems (Ga, Bi, Si etc) could not be so readily understood. Further high-P, T melting experiments found even more unusual behaviour, for a very wide range of systems that extended from the metallic elements (Cs, Rb, Ba and Eu), via chalcogenide and halogen semiconducting elements (Se, Te, Sb, I), to ionic or H-bonded compounds (KNO_3, KNO_2, Li_2CrO_4, Na_2SeO_4, Bi_2Te_3, $NaClO_3$, KH_2AsO_4): these all exhibited one or even several *maxima* occurring in their melting curves [11, 17]. Elemental carbon has now been shown to possess melting curve maxima for both its graphite and diamond forms [16, 18–20]. These observations indicate that unusual and unexpected densification mechanisms can be operating in the liquid state of matter.

A solution to the melting curve problem was first proposed by Rapoport, that was based on earlier ideas developed for H_2O by Klement [17]. It had been suggested that liquid water might contain distinct structural states, species or domains, depending upon the presence or absence of H-bonding between the H_2O molecules. In particular, there could exist (a) open-structured low-density regions locally analogous to crystalline ice polymorphs versus (b) higher-density domains containing randomly packed H_2O molecules. The species should interconvert rapidly via fast rearrangement of the H-bonding patterns and hopping of H^+ ions, to give rise to 'flickering cluster' models of the liquid structure often described in physical chemistry texts [21–23]. The time- and spatially averaged relative proportion of low- versus high-density species should be constant for a given set of P, T conditions, but would be expected to change as a function of the pressure or temperature. Rapoport applied the two-species concept to understand the unusual melting behaviour observed for certain systems at high P [17]. To provide a structural basis for his argument, he presumed that the liquids might contain local structures or packing arrangements that could be analogous to those found in corresponding low- versus high-pressure crystals. There is a wide variety of such examples among all structure and bonding types. For example, Rapoport noted that low-density phases of Cs, Ba and Eu contain bcc packing with the metal atoms in eightfold coordination. At high P, the crystals change to fcc or hcp structures, with the atoms in 12-fold coordination [11, 17]. Low-pressure Te contains spiral chains, whereas high-P crystals have the β-Po structure with atoms in 6-coordination. In low-pressure KNO_3-I, the cations make contact with a single O^{2-} of the planar NO_3^- group; in high pressure KNO_3-III, the K^+ ion is bound to two oxygens, and the NO_3^- anion is no longer free to rotate [17].

Rapoport proposed that the low- and high-density domains in the liquids could represent regions with similar coordination environments to those found in the corresponding crystals. However, in contrast to the crystalline phases, both the low- and high-density local species or domains would be present simultaneously in the liquids at a given density. The relative proportion of such high- versus low-density states in the amorphous state could change continuously as a function of P, unlike the case for crystals, in which all atomic environments must change simultaneously at a transition pressure, to maintain the long-range translational symmetry. The result is that a two-state liquid can increase its density (i.e. expressed as the inverse of the molar volume, $1/V$, at constant T) more rapidly than would be expected from the compressibility of a single set of structural units. In some circumstances, it could be expected to achieve a higher density than the underlying crystal. That consideration leads to a general argument for the appearance of the melting curve maxima. They also provide an explanation for the negative initial melting slopes observed in some systems, that then imply a maximum occurring in (dT_m/dP) at 'negative pressure', i.e., in a tensile-strained regime [1, 24]. Rapoport analysed the generalized melting relation for the two-state liquid

at high P using the thermodynamic formalism of a 'regular solution' model, that had recently been suggested to describe liquid mixtures [25], to obtain the Gibbs' free energy for the liquid state. In his 'two-state' or 'two-domain' model, he considered the low- (A) and high-density (B) 'species' or 'domains' to constitute thermodynamic mixing components in the liquid.

Within the simpler 'ideal' solution model developed to describe liquid mixing, it was presumed that any contributions to the mixing energy arise from the configurational entropy. This type of model works well for systems in which the components are chemically and structurally similar (e.g. C_6H_5Cl versus C_6H_5Br). However, in most systems, there is usually an enthalpy penalty (or gain) that is associated with formation of liquid mixtures or solutions [25]. Rapoport assumed that such a ΔH_{mix} term would also arise from the simultaneous presence of the low- and high-density species or domains within the two-state liquids described by his model. The overall Gibbs free energy is determined as a sum of the partial molar free energy contributions associated with low- and high-density components, i.e.

$$G = X_{\mathrm{A}} G_{\mathrm{A}} + X_{\mathrm{B}} G_{\mathrm{B}}. \tag{2}$$

Here X_{A} and X_{B} are the mole fractions of the low- and high-density 'species', respectively. Their partial molar contributions to the Gibbs energy are, respectively,

$$\begin{aligned} G_{\mathrm{A}} &= G^0_{\mathrm{A}} + V^0_{\mathrm{A}}(P - P_0) + RT\ln(X_{\mathrm{A}}) + W(1 - X_{\mathrm{A}})^2 \\ G_{\mathrm{B}} &= G^0_{\mathrm{B}} + V^0_{\mathrm{B}}(P - P_0) + RT\ln(X_{\mathrm{B}}) + W(1 - X_{\mathrm{B}})^2. \end{aligned} \tag{3}$$

Here, P_0 is a standard state pressure (usually $P_0 = 1$ atm); G^0_{A} and G^0_{B} are the partial molar free energies of species A and B corresponding to the standard state at P_0, V^0_{A} and V^0_{B} are the respective standard molar volumes (that are usually modelled using from data on crystalline polymorphs [1, 17, 26–29]) and R is the universal gas constant (8.314 J mol^{-1} K^{-1}). W corresponds to a regular solution 'interaction parameter' that has dimensions of energy and that expresses the magnitude of the excess enthalpy contribution that arises in the liquid system due to the simultaneous presence of two (or more) components. The excess Gibbs energy of mixing for a two-state liquid is then written as

$$\begin{aligned} \Delta G_{\mathrm{mix}} = {} & RT[X_{\mathrm{A}}\ln X_{\mathrm{A}} + (1 - X_{\mathrm{A}})\ln(1 - X_{\mathrm{A}})] + P\,[X_{\mathrm{A}}V_{\mathrm{A}} + (1 - X_{\mathrm{A}})V_{\mathrm{B}}] \\ & + X_{\mathrm{A}}(1 - X_{\mathrm{A}})W. \end{aligned} \tag{4}$$

Such expressions for the free energy of the two-state liquid permit T_{m} to be evaluated as the locus of crystal–liquid equilibrium points, as a function of the pressure. Approximate values for V^0_{A} and V^0_{B} are usually estimated from crystalline data. Other versions of the two-state or two-species models have now been developed and applied to various classes of liquids and amorphous solids; for example, a 'bond lattice excitation' model was developed to describe tetrahedrally coordinated systems such as H_2O, SiO_2, BeF_2, Si and Ge [30, 31]. In this case, a model lattice or network of covalent bonds was constructed and presumed to become locally 'excited' via bond-breaking and reformation events. Other local 'excitation' models involving cooperatively relaxing domains have also been described and applied to molecular systems [8, 32, 33].

In general, it is not expected that the modelled low- and high-density species or domains should actually correspond to any crystalline structures or even to local structural units observed in crystals: it is well known that various coordination and bonding environments that are not represented among crystals can occur within liquids and glasses. Also, it is expected that rapid interchange can occur between the low- and high-density species present within the liquids, so that it is the dynamically averaged structures that are present in the relative proportions set by the P or accessed at various T values. However, the simple two-state picture provides a useful starting model for understanding and calculating the unusual liquid properties within

polyamorphic systems, and for visualizing the different structural species and bonding or coordination environments that might be present. However, the actual structures present within a given system must be determined by a combination of experimental studies and theoretical simulation. This goal presents a major challenge for liquid state simulations along with x-ray and neutron scattering studies, that is described here.

During studies of the excess free energy of mixing obtained as a function of the mixing enthalpy parameter, Rapoport expressed the mixing term as w/kT, where $k = R/N_A$, with N_A Avogadro's number. Within conventional liquid mixtures where X_B is the mole fraction of a second chemical component, the condition $w/kT = 2$ represents a critical point in the system, beyond which compositional unmixing into two liquid phases occurs [25]. Likewise, Rapoport's two-state liquid developed a double minimum in $\Delta G_{mix}(X_B)$ for $w/kT > 2$, where X_B is now the mole fraction of high- versus low-density species. This result indicated that phase separation could occur in the liquid *at constant chemical composition*, between discrete liquid phases with low- and high-density values. In his pioneering paper, Rapoport noted that '*the value* $w/kT = 2$ *is a critical one and larger values lead to separation into two phases*'. However, he did not pursue the argument: '*... such separation into two liquids has, as yet, never been encountered and we therefore restrict ourselves to values of* $w/kT < 2$' [17] (figure 1).

A direct experimental observation of a liquid–liquid phase transition occurring at constant chemical composition between distinct liquid phases with different densities was only made ∼30 years later, when the phenomenon was observed to occur within supercooled liquids in the Y_2O_3–Al_2O_3 system [34] (figure 2). However, the likely presence of a density-driven liquid–liquid phase transition in supercooled liquid water had already been indicated by experimental work on polyamorphism in solid amorphous H_2O, and from MD simulation results [2, 9, 33, 35–39]. The L–L transition observed in undercooled Y_2O_3–Al_2O_3 liquids was particularly interesting, because that system had the capacity to undergo compositionally driven unmixing, but it did not: the primary driving force for the liquid–liquid phase transition is thus due to density or entropy gradients developed within the system. Recent experiments on liquid phosphorus using x-ray scattering carried out under high-P, T conditions have now indicated a liquid–liquid (L–L) transition occurring above the melting line, in the stable liquid regime [40–43]. However, recent work suggests that the transition in fact occurs between a high-density polymeric liquid and a low-density monomeric fluid phase [42]. This situation highlights the fact that each liquid polyamorph is expected to possess its own critical point, for the liquid–gas–fluid equilibrium. Likewise, each low- or high-density liquid polyamorph will have a separate glass transformation range (i.e. T_g^L, T_g^H), and this must be taken into account when designing probe experiments and analysing the data.

Density-driven L–L transitions have also been suggested to occur in liquid S, Se, Te and I, based on dramatic changes observed in the electrical conductivity, viscosity, density etc, as a function of P and T [6, 44, 45]. However, it is not yet clear whether these effects correspond to actual phase transition behaviour, or to rapid changes in the physical properties of the liquid within the one-phase regime, above T_c. Another polyamorphic transition has been described for the organic salt triphenyl phosphite (TPP), based on differential scanning calorimetry (DSC) observations combined with other physical measurements, and theoretical modelling [32, 46–51].

The temperature of the critical point (i.e. $T_c = T_{crit,L-L}$), below which a one-phase, two-state liquid transforms into a two-phase system exhibiting an L–L phase transition, is determined by the magnitude of the mixing enthalpy, ΔH_{mix} or W. Generally, it is expected that $W < \Delta H_{melting}$ (that determines the melting temperature, T_m) because the relative enthalpic contributions for bonding rearrangements between low- and high-density liquid polyamorphs are usually expected to be smaller than those between crystals versus liquid states [3]. It follows

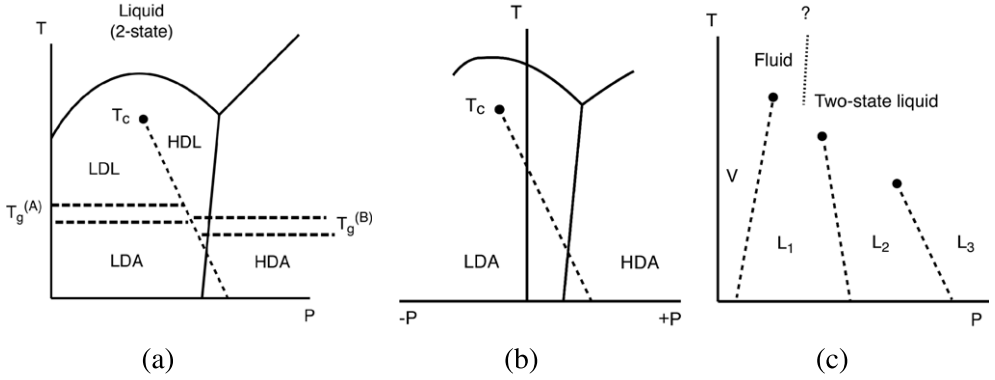

Figure 1. Generalized P–T phase diagrams indicating the relationship between the two-state model and the development of density-, entropy-driven liquid–liquid phase transitions at constant composition. (a) A maximum occurring in the melting curve is explained by development of a 'two-state' model for the liquid structure. The liquid contains distinct 'species' or rapidly fluctuating domains, that have different coordination numbers or bonding patterns, that result in differences in the density and/or the entropy. An increased proportion of high-density domains as a function of increased pressure explains the turnover in the melting slope above the lower density crystalline phase. If crystallization is bypassed upon cooling, a critical point (T_c) is encountered. Below this P, T point, the liquid develops a double minimum in its free energy of 'mixing' between low- and high-density components, causing separation into low- and high-density liquid polymorphs (LDL, HDL), separated by a first-order phase transition line. Thermodynamic arguments indicate that this line is most likely to have a negative dT_{LL}/dP slope [3]. The LDL and HDL liquids are generally expected to have different glass transitions ($T_g^{(A)}$ and $T_g^{(B)}$), indicated schematically as dotted ranges; in fact, the T_g values will increase or decrease with P, tracking the melting lines. Below T_g, the supercooled liquid phases transform into the non-ergodic LDA and HDA amorphous states. Versions of HDA and LDA polyamorphs can also be produced by other methods, including pressure-induced amorphization [1, 4, 39]. (b) In cases for which a negative initial melting slope is observed, such as Si, Ge and H_2O, the maximum in the melting curve is expected to occur at 'negative pressure', i.e. in a metastable tensile regime where the ground state for the system is the vapour phase. (c) In any liquid system exhibiting polyamorphism, a series of density-, entropy-driven phase transitions might be generally expected as a function of P and T, between liquid phases with distinct structures and thermodynamic and physical properties. At lowest density, the first of these amorphous–amorphous transitions is thus the liquid–gas transition. Above the gas–liquid critical point lies the fluid state of matter. An as-yet unexplored region for *in situ* high-P–T studies lies between the fluid and multi-domain liquid states, beyond the critical points for all phases. Studying such behaviour represents a challenge for experimental and theoretical studies.

that density-driven L–L transitions are generally expected to occur within the metastable supercooled liquid state, often well below T_m [4, 5, 8, 9, 36, 38, 52–55]. This observation leads to significant challenges for both experimental and theoretical investigations of the phenomena.

The structural states of low- and high-density polyamorphs are determined by diffraction studies, using x-ray and neutron scattering to determine the structure factor ($S(Q)$) as a function of P and T. X-ray absorption combined with analysis of the EXAFS region is also used to study liquid- and glassy-state polyamorphism [56–61]. The analysis and interpretation of amorphous x-ray or neutron diffraction data is already challenging for samples measured at ambient conditions [62, 63]. However, experimental investigations of structural changes associated with polyamorphism generally require amorphous scattering studies to be carried out *in situ* at high P, using diamond anvil cells (DACs), or in large-volume devices such as the multi-anvil device or Paris–Edinburgh cell [39, 41, 42, 63–77]. This greatly increases the level of difficulty in obtaining and analysing the experimental data sets [63, 68, 78, 79]. The available Q range in such high-P studies is often severely limited by geometrical constraints,

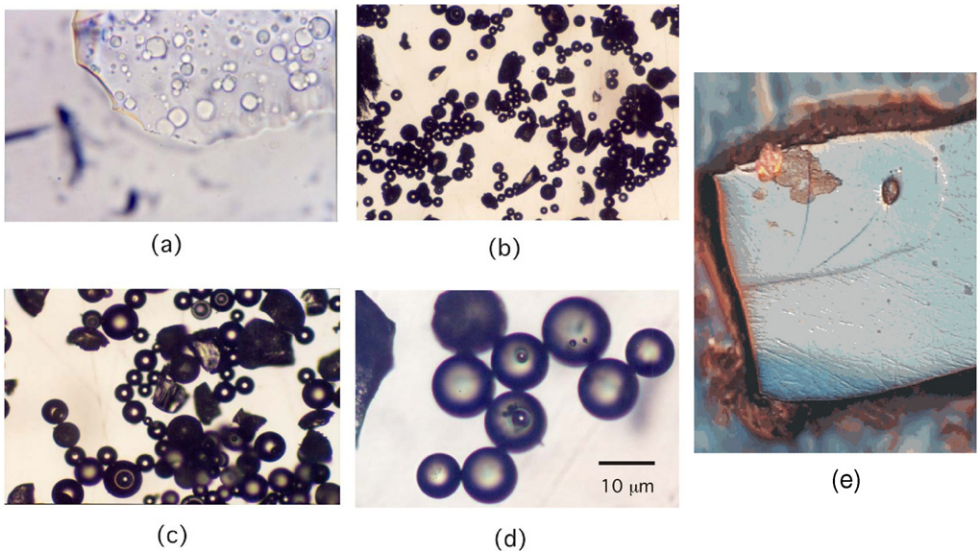

Figure 2. A density-, entropy-driven liquid–liquid phase transition is encountered during quenching supercooled Y_2O_3–Al_2O_3 liquids. Spherical inclusions of an LDL phase nucleate and grow within the HDL liquid, and both are recovered as metastably coexisting glasses by rapid quenching. (a) Photomicrograph of a Y_2O_3–Al_2O_3 glassy sample containing 23 mol% Y_2O_3 recovered from a roller quench experiment (field of view ∼200 μm). Sub-spherical glassy inclusions that nucleated and grew during the quench are clearly visible within the glassy matrix; some of the inclusions clearly show evidence for 'necking' and other features that indicate they originated in the molten state. The LDA and HDA polyamorphs are distinguished by their optical and mechanical properties, and by DTA/DSC calorimetry experiments [53, 54, 117, 119, 120]. (b) Photomicrograph (field of view 300 μm) of glassy 'beads' along with irregular shards of matrix glass, following mechanical separation of the two amorphous 'phases'. (c) A closer view of the separated glassy beads and matrix material. Conchoidal fracture surfaces on matrix glass fragments are clearly visible. Most of the 'beads' (i.e. derived from the glassy inclusion phases) are perfectly spherical, but some have 'dimples' on their surface, or they contain a cavitation void within the interior, indicating volume relaxation during the quench. (d) A close-up view of several separated glassy 'beads' (the edge of a 'matrix' glass shard appears on the left). Five of the beads are solid and perfectly regular, and three show circular 'voids' at their surface, that correspond to those that appear within the interior. One bead at the top has crystallized, and this forms an opaque mass with an irregular outline. (e) Larger samples of Y_2O_3–Al_2O_3 glasses can be formed by high-T melting in a Xe lamp thermal imaging furnace, and quenched by passing the molten droplets through a Pt wire grid. Here, the polished sample shows coexisting LDA (top left) and HDA matrix regions. The glassy polyamorphs have different mechanical properties, resulting in a higher quality of polish for the LDA sample. Aliquots of such samples are prepared for neutron and x-ray scattering experiments, as well as calorimetry studies [92, 117].

and scattering contributions from the diamond windows or other sample containment materials must be evaluated and eliminated from the data sets. Studies of polyamorphism in supercooled liquids are also carried out at high T and ambient P using levitation techniques; use of these methods brings in experimental challenges associated with maintaining stable levitation regimes within the synchrotron or neutron beam [63, 80–84]. Finally, *in situ* studies of L–L phase transitions and the structural changes accompanying polyamorphism under combined high-P, T conditions, or at high P and cryogenic low T, pose additional sets of experimental constraints and challenges [39, 41, 63, 71, 73, 85].

Molecular dynamics (MD) theoretical simulations are used extensively in fundamental studies of polyamorphism and L–L transitions, and the results are also used to interpret experimental x-ray and neutron scattering data obtained on polyamorphic

systems [3, 28, 31, 36–39, 55, 64, 75, 86–100]. Simulation techniques are also useful to study the onset of anomalous physical behaviour in the one-liquid phase regime above T_c, that might be associated with the onset of L–L transitions at lower T [9, 31, 36, 38, 94–97, 99, 101, 102]. It is possible to study anomalous fluctuations in the equilibrated simulation system volume (V) at sufficiently long simulation timescales, to indicate sampling of low- versus high-density states within the single-phase liquids above T_c [28, 75, 91, 92].

However, the nature of the polyamorphism problem also means that significant challenges are present for theoretical investigations. It is difficult to design and implement appropriate potential energy functions to treat the wide variety of polyamorphic systems, when the low- and high-density liquids or polyamorphs can have very different bonding characteristics and electronic properties. Simulation approaches based on *ab initio* or first-principles electronic structure methods should provide a general solution to this problem; however, the system sizes available to date are often quite small and this can substantially affect the interpretation of results. It is most useful to use very long simulation times combined with the largest system sizes to study the occurrence and onset of polyamorphic behaviour, especially since T_c for L–L transitions generally lies at low T, in an undercooled regime well below the melting line. MD simulation approaches to the problem will ultimately require 'million-atom'-scale simulations, in order to produce a system that is large enough to observe the nucleation of nanoscale regions within the liquid. However, satisfying these conditions requires the use of the most advanced simulation techniques and computing technology, even within the context of 'classical' simulations. The emerging application of *ab initio*/first-principles simulation techniques will move towards resolving the problem of designing appropriate potential functions that can adequately model the bonding in the system; however, the large computational resources required for such calculations are at or beyond the limit of current computational methodologies. However, rapid advances being made in the implementation of large-scale national and international computing networks with massively parallel capabilities combined with advanced algorithms are expected to result in major advances in the understanding of polyamorphic systems, including supercooled liquid behaviour and the properties of solid amorphous states. Other large-scale simulation approaches to address the polyamorphism problem are also being developed [103].

1.2. Polyamorphic transformations in the solid amorphous state: pressure-induced amorphization and polyamorphism of H_2O

Another way to approach the understanding of phenomena related to density-driven L–L phase transitions is via studies of the solid amorphous state at high pressure [1]. The now-classic series of studies on the polyamorphism of amorphous H_2O began with an experimental study of pressure-induced amorphization (PIA) of the ice Ih crystalline phase. As noted previously, this compound has unusual melting behaviour, with negative dT_m/dP at $P = 1$ atm. It was hypothesized that if the crystal were compressed at sufficiently low T to preclude crystalline phase transitions it should encounter a metastable extension of its melting curve and spontaneous transformation to an amorphous state would occur. The phenomenon is analogous to a melting relation, but because it occurs below T_g it results in a solid amorphous state. This experiment was first carried out, and the first demonstration of the PIA phenomenon was recorded for ice Ih at $P = 0.9$ GPa and $T = 77$ K, by Mishima and co-workers [104]. It was immediately noted that the process resulted in a new high-density amorphous form of H_2O (HDA), that was different from the low-density (LDA) a-H_2O normally produced by vapour-phase condensation [35, 38, 104, 105]. Mishima *et al* showed that the HDA polyamorph underwent an apparently first-order transformation into the

LDA polyamorph on heating the metastably recovered HDA polyamorph to $T > 117$ K at $P = 1$ atm [35, 38, 39]. Calorimetry studies and P–T cycling experiments allowed the authors to map out the likely locations in P–T space of the first-order LDA–HDA transition boundary and its associated spinodal lines, that represent the intrinsic stability limits of the HDA and LDA polyamorphs to low and high densities [9, 106–108]. The observed transition between HDA and LDA polyamorphs of solid-state a-H_2O was extended upwards in T to make contact with an analogous density-driven L–L phase transition in supercooled liquid water (between corresponding HDL and LDL liquid phases), that had been predicted from thermodynamic analyses and MD simulations [9, 36–39, 108]. The existence of the low- versus high-density spinodal lines between HDA and LDA polyamorphs during high-P, T cycling experiments has recently been confirmed by Nelmes *et al*, using neutron diffraction measurements of $S(Q)$ to distinguish between the a-H_2O polyamorphs [71]. These are conveniently referred to the position of the first obvious peak in the scattering function, that is often converted to an effective distance or 'd spacing' via $Q = 2\pi/d$ [39, 71, 105]

It is important to recognize that the solid amorphous HDA form as produced by PIA is not in an internally thermally equilibrated state, and it is not necessarily structurally identical to a corresponding hypothetical glass that would be produced by rapid cooling from the supercooled liquid under high-pressure conditions, although the two could be expected to be related. Nelmes *et al* carried out annealing experiments to relax the HDA structure at high pressure [71]. Upon recovery to ambient P, the HDA polyamorph has become highly metastable with respect to the LDA form, and the two are likely to be related by a first-order-like transition that maps on to the expected LDL–HDL phase transition expected to occur in the supercooled liquid state [9, 23, 36–39, 108]. Various events can occur during heating HDA at ambient P, that depend upon the heating rate and the structural state of the sample, even assuming that metastable crystallization is avoided. Obviously, as the T is raised, the sample will begin to relax structurally, and the $S(Q)$ measurements can give an indication of T_g [38, 39, 71, 109]. Heterogeneous nucleation and growth of the LDA polyamorph can occur via a first order process, or if the initial sample is well equilibrated it can be superheated to near the spinodal limit, at which point spontaneous density fluctuations appear throughout the material. All of these processes can give rise to static and dynamic heterogeneities resulting in small-angle neutron or x-ray scattering signals [69, 70].

A further complication has arisen recently regarding the interpretation and nature of polyamorphism in a-H_2O with the identification of a new 'very high-density' amorphous (VHDA) form of a-H_2O, produced at $P > 1.1$–1.9 GPa [38, 39, 72, 110–112]. Like HDA, the VHDA polyamorph can be recovered metastably to ambient conditions, and it also undergoes transformation during heating to LDA-a-H_2O. It has been suggested that VHDA represents a 'relaxed' form of the HDA polyamorph, and that transformations between VHDA–HDA–LDA could be continuous rather than related to an underlying density-driven L–L phase transition [39, 72, 111]. However, the HDA–LDA transition hypothesis is fully supported by the P, T cycling experiments of Nelmes *et al*, using annealed materials, that corroborate the earlier findings of Mishima *et al* in determining the location of the low- and high-density spinodal boundaries that must be associated with a first-order phase transition line [9, 71, 107, 108]. The relationship between HDA and VHDA is not yet clear. It could well be the case that a second density-driven transition is present between HDA and VHDA polyamorphs [38, 39, 71, 110]. Just as in crystalline polymorphism at high P and high T, we should expect a series of liquid–liquid phase transitions to be present for a given substance as a function of the density, with the lowest-density transition corresponding to the liquid–gas transition [3, 7] (figure 1).

Fully understanding the metastable phase diagram of supercooled liquid H_2O and its extension into the solid amorphous state as a function of P and T represents continuing

challenges for experimental x-ray and neutron scattering combined with calorimetry and spectroscopic techniques, and computer simulation/modelling using empirical potentials and *ab initio* techniques. The experiments carried out to date have set the agenda for these studies: it is critically important to fully specify and control the state of structural relaxation within the initial sample, and to determine the rate of change of the P, T conditions during investigations of the VHDA–HDA–LDA transformations. Elastic and inelastic $S(Q)$ determinations by neutron and x-ray scattering measurements in both the wide- and small-angle regime are necessary to explore the structural and dynamic changes within the samples and observe the onset of phase transition behaviour in the metastable regime. One challenge for the experiments is that the starting high-density a-H_2O samples must be produced via the PIA technique, that does not initially yield fully equilibrated materials. MD simulation approaches to the problem are mainly limited by the sophistication of potential energy functions that can be applied to a system that contains both strong covalent interactions between O and H and weaker H-bonding interactions, as well as potential ionic contributions from $H^+/(H_nO_y)^+ \cdots$ OH pairs. However, *ab initio* simulations that are expected to be implemented using advanced computational techniques combined with massively parallel processing and networking technologies will relieve this problem. This provides another grand challenge for liquids and amorphous systems in general, as well as addressing the problem of polyamorphism.

1.3. The polyamorphic behaviour of chalcogenide and pnictide liquids at high-T and high-P conditions

It is well known that elemental liquids such as S, Se, Te, P and I exhibit large and rapid changes in their physical properties at high T and high P, including anomalous changes in the viscosity and electrical conductivity, and discontinuities observed in the melting curves [11, 44, 45, 113, 114]. Dramatic changes are observed in the liquid and glassy structures as a function of pressure and temperature, and it has been suggested that density-, entropy-driven L–L phase transitions might be present [6, 40–42, 44, 45, 73, 74, 113]. It has also been proposed that the changes in physical properties could be due to dynamic nanoscale domain formation in the one-phase liquids above T_c [6, 44, 45].

Even the crystalline polymorphism in these materials is not yet completely determined. At ambient P, they form two- or three-connected networks linked by covalent bonds into various ring, chain and cluster configurations, that form molecular structures linked by weak van der Waals' interactions. A wide range of polymorphs have been described for S and P, most of which have not yet been completely characterized, even at ambient P [114]. It is generally agreed that orthorhombic α-S_8 is the thermodynamically stable form of the element at ambient P and T; however, other metastable varieties are known to persist over wide T–P ranges. White phosphorus containing isolated P_4 tetrahedra is a common allotrope of the element, but it is thought to be thermodynamically metastable relative to some 'red' polymorph. However, all known 'red' or 'brown' varieties of the element are amorphous, and hence they must be metastable relative to some as yet unidentified crystalline form. In the various melting curve determinations for the chalcogenide or pnictide elements, it is not always certain that the most appropriate melting relations have been measured [42].

The unusual behaviour of liquid sulphur at ambient P is a classic case in inorganic chemistry. Heating the α-orthorhombic crystalline allotrope to above 95.3 °C causes transformation into a β-monoclinic polymorph that also contains S_8 rings; however, the α-form may persist metastably to higher temperature. The metastable melting point for α-S_8 lies between 112.8 and 115.1 °C, and that for β-S_8 is 114.6–120.4 °C, depending upon the crystallite size. It is known that S_8 ring opening reactions begin to occur at ∼119 °C, forming

oligomeric species that can depress the melting point. Immediately upon melting, a pale yellow liquid is obtained that has low viscosity, due to the low energy barriers impeding relative motion of the S_8 rings. Remarkably, the viscosity initially *increases* upon heating to reach a maximum at ∼200 °C and the colour deepens to dark red–brown [114, 115]. It is determined that ring-opening reactions give rise to oligomeric $-(S)_n-S$ oligomeric radical species that that concatenate, affecting the viscosity and colour. The specific heat and other physical properties exhibit a sharp discontinuity termed the 'lambda' transition after its shape in the DSC trace at 159.4 °C. Such a transition is typically associated with a second-order phase transition that is driven by phonon, elastic or electronic instabilities in crystalline solids. It is obvious that a rapidly increasing number of ring opening, S–S bond breaking, and concatenation reactions occur with T in this range. However, it is not yet certain that the behaviour of sulphur constitutes evidence for occurrence of a true thermodynamic L–L phase transition of the second order in the liquid state at high T.

The white phosphorus polymorph containing P_4 units transforms into a metallic black form at $P = 1.2$ GPa, that has a polymeric structure based on interwoven zigzag chains of three-connected P atoms in pyramidal coordination. Recently, it has been determined from a combination of *in situ* x-ray scattering and imaging experiments that a first-order phase transition occurs above the liquidus at $P \sim 1.0$–1.2 GPa [40–42]. This remarkable finding seemed to provide a first case in which a density-driven L–L phase transition was documented in the stable liquid field [43]. However, careful analysis of the stable and metastable thermodynamic relations has indicated that the low-density molecular phase is in fact above its liquid–gas coexistence point, and it thus constitutes a fluid state. The true liquid only appears at much lower T, below the melting line [42].

It is obvious that understanding the stable and metastable melting relations, and the possible existence of multiple density- or entropy-driven L–L phase transitions, that likely occur among chalcogenide and pnictide systems represents a major challenge for *in situ* experiments using neutron and x-ray scattering under combined high-P, T conditions [40–42]. There are also major theoretical challenges for studying these systems that contain a mixture of covalent and van der Waals' bonding, and in which the properties change rapidly from insulating and semiconducting to metallic as a function of the density, using simulation methods that can accurately capture the features of the polyamorphic changes [42, 90]. The importance of studying polyamorphism and L–L phase transitions in these systems extends beyond the elements. Polymeric liquid mixtures are formed over wide compositional ranges in systems such as S–Se–Te–As–P etc, and extending to include tetrelides and halides (Ge, Si, I, Br, etc). Many of these molten systems are glass forming, and they give rise to technologically important families of semiconducting and photoactive glasses and amorphous solids [116]. Compositionally driven unmixing is also well known to occur among these systems, for example along the join Ge–$GeSe_2$. However, both of these end-member compositions have been reported to exhibit density-driven polyamorphism, or liquid–liquid transitions. They will thus constitute a test ground for understanding the interplay between the thermodynamic parameters of density ($\rho = 1/V$), entropy (S) and chemical composition (X), acting in response to the variables of pressure (P), temperature (T) and chemical potential ($\mu(X)$), in effecting liquid-state phase transitions.

1.4. The case of Y_2O_3–Al_2O_3: direct observation of a density-driven L–L transition occurring in the supercooled liquid state

The first direct observation of a density liquid–liquid phase transition that corresponded to Rapoport's prediction was made by Aasland and McMillan, following a study of supercooled

liquids in the Y_2O_3–Al_2O_3 system [34, 53, 54, 64, 117] (figure 2). During hot-stage microscopy studies originally designed to observe melting/recrystallization events, a new low-density liquid phase was observed to nucleate and grow within the high-T liquid during quenching experiments in the supercooled regime. The L–L transformation was arrested during glass transformation, so that samples of both liquids were recovered as metastably coexisting glasses. These were determined to have experimentally identical chemical compositions, but they had different densities and structural parameters as determined by neutron and x-ray scattering measurements, as well as Raman and IR spectroscopy, observation of mechanical properties, and thermodynamic studies of the enthalpy and entropy [34, 53, 54, 64, 83, 91, 92, 117–120]. New results on MD simulations of the density fluctuations developed within the one-phase liquid above T_c are given below, along with recent data on x-ray scattering experiments carried out in the supercooled liquid regime during levitation experiments.

1.5. Density-driven structure changes and 'polyamorphism' in network glasses: SiO_2 and GeO_2

Large changes are observed to occur in the structure and physical properties of amorphous SiO_2 and GeO_2, as well as related network glasses such as BeF_2, $ZnCl_2$, $GeSe_2$, etc, either studied *in situ* at high P or following recovery of 'permanently' densified samples to ambient pressure [31, 61, 121–134]. It has long been known that glasses and amorphous solids can be produced within these systems by various methods including chemical vapour deposition, sol–gel synthesis etc, and that the structure and physical properties of the amorphous materials depend upon the method of preparation as well as subsequent pressurization or heat treatment. Such observations gave rise to early concepts of 'polymorphism' within the solid amorphous state, independent from possible links to an underlying density-driven liquid–liquid phase transition, that emerged later [4, 5, 9, 34, 61].

The terminology associated with the new field of amorphous and liquid state studies emerged at approximately the same time, based on studies in different systems. Large structural changes were observed during densification of vitreous SiO_2, and they were suggested by Grimsditch to be associated with transformations occurring between distinct glassy states: a phenomenon that he described as 'amorphous polymorphism' [135, 136]. The term 'polyamorph' was first used by Wolf to designate the low- and high-density forms observed to occur for the analogous glassy compound a–GeO_2 [121], and a two-state model was developed to describe the transformations between the two forms of the amorphous material [121, 133]. At low P, both SiO_2 and GeO_2 glasses and their low-density crystalline polymorphs possess open framework structures dominated by tetrahedral TO_4 units (T = Si, Ge) interconnected by T–O–T linkages. Applying high P (e.g. >9–10 GPa) to SiO_2 results in transformation to six-coordinated polymorphs such as stishovite. The analogous rutile-structured phase of GeO_2 is stable at ambient P, T conditions, but its four-coordinated quartz form is stabilized at high T. The low-density glass and liquid appear to contain linked GeO_4 units. From static and shock wave compression experiments, the $V(P)$ relations of SiO_2 and GeO_2 glasses at low P parallel those of the tetrahedral crystalline solids. Above $P = 8$–10 GPa, there is an abrupt increase in the density, and the $V(P)$ curve at high P approaches that of the six-coordinated crystalline phases [68, 89, 121, 123, 131, 133, 137–140]. *In situ* XAS and EXAFS experiments, IR and Raman spectroscopic studies, and x-ray amorphous scattering measurements indicate that the coordination number in SiO_2 and GeO_2 glasses increases abruptly in this pressure range [58, 68, 121, 123, 131, 133, 141, 142]. The large structural changes with pressurization are reflected in the results of MD simulations [89, 93]. The PIA observed in the systems could be related to melting curve behaviour, and there could be an underlying density-driven

liquid–liquid phase transition present [1, 3–5, 7, 94, 95, 97, 101, 121, 131, 133, 140, 143]. There is a formal analogy of these effects for SiO_2 and GeO_2 with the HDA–LDA phenomenology observed for H_2O [31, 93, 121–123, 140, 143].

A future challenge for experimental and theoretical investigations of polyamorphism is to fully elucidate the structural changes occurring in glassy and molten SiO_2, GeO_2 and other tetrahedral glass-forming liquids and amorphous solids by *in situ* scattering studies at high P and at high T, and to determine whether these can be linked to the postulated density-, entropy-driven L–L phase transitions. As for H_2O, a-Si and a-Ge, and chalcogenide–pnictide systems discussed above, it will also be particularly important to determine whether a *sequence* of density-driven L–L transitions might be present as a function of increasing density [3, 7, 44] (figure 1). Also, as for the Ge–$GeSe_2$ system described above, systems such as SiO_2–Na_2O and SiO_2–CaO exhibit well known phenomena of liquid- or glassy-state unmixing into chemically distinct end-members [144]. In future, it will be of great importance to study the relative role of density-, entropy-driven L–L phase transitions and polyamorphism, compared with that driven by gradients in the chemical potential.

2. Y_2O_3–Al_2O_3 supercooled liquids and glasses: neutron and x-ray scattering experiments and MD simulations

Following the experimental observation of the L–L phase transition in Al_2O_3–Y_2O_3 supercooled liquids, it was determined that the compositions of the coexisting glasses were identical within experimental error, and that the LDA and HDA glasses differed by ∼4% in their density [34, 53, 54, 64, 117, 120]. Development of a new quench technique combined with use of an Xe lamp thermal imaging furnace permitted us to prepare large enough samples to carry out calorimetry experiments, that allowed us to observe the enthalpic signature of the L–L transition and also the independent glass transformations of the LDA and HDA polyamorphs [53, 54, 117]. Then the challenge was to determine the nature of the structural differences between the two polyamorphs, that would give rise to the differences in density and entropy recorded between them, and allow an insight into the thermodynamic driving forces responsible for the L–L transition. We must note that this remains an ongoing problem despite extensive series of x-ray and neutron scattering experiments and MD simulations, although it appears that the origin of the polyamorphism lies in the next-nearest-neighbour packing of metal ions (i.e. the Y . . . Y, Y . . . Al distributions) and the relative connectivity and clustering of YO_n and AlO_4 polyhedra.

The availability of large samples for the calorimetry studies also permitted us to carry out neutron and x-ray scattering experiments. The neutron scattering data were obtained first using the GLAD instrument at IPNS (Argonne National Laboratory, IL, USA), and then SANDALS at ISIS (Rutherford–Appleton Laboratory, UK) [92, 118] (figures 3 and 4). The data obtained at the ISIS spallation source allowed us to observe correlations over a very large Q range (up to 40 $Å^{-1}$), thus greatly improving the resolution of the Fourier transformed real space distribution functions (figure 4). Also, the second series of samples prepared for the ISIS studies contained fewer crystallites than those initially studied at IPNS, so that the observed scattering contained fewer Bragg reflections that complicated the analysis and interpretation of the glassy data. In a further series of experiments, we also obtained complementary high-energy synchrotron x-ray scattering data (out to $Q \sim 20$ $Å^{-1}$) at beamline ID-11 (BESSRC) at the Advanced Photon Source (Argonne National Laboratory, IL, USA) [92] (figure 3).

The HDL–LDL transition temperature (T_c) in the Al_2O_3–Y_2O_3 system decreases with Y_2O_3 content [34, 120]. Because of this, we could prepare samples for calorimetry and for

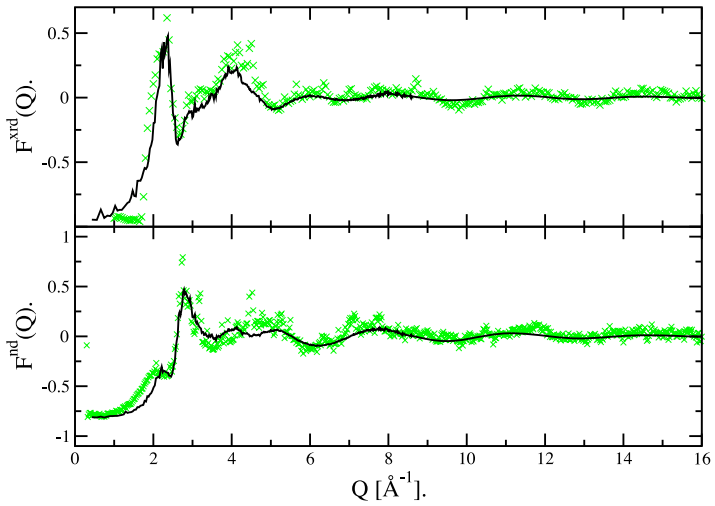

Figure 3. Experimental (crosses) and calculated (solid line) x-ray (upper panel) and neutron (lower panel) total scattering functions for a polyamorphic Y_2O_3–Al_2O_3 glass composition with 20 mol% (AY20). High-energy synchrotron x-ray data were acquired at beam line 11-ID-C of the Advanced Photon Source (Argonne National Laboratory, IL, USA). Neutron diffraction experiments were carried out on the GLAD instrument at the Intense Pulsed Neutron Source, Argonne National Laboratory, and at SANDALS, ISIS spallation source, Rutherford–Appleton Laboratory, UK. The many-body ion dynamics simulation results were generated from a run equilibrated at a constant temperature of 2400 K over 2.2 ns of simulation timescale [54, 64, 91, 92, 118].

the neutron and x-ray scattering studies that contained different proportions of the HDA and LDA polyamorphs by quenching at a similar rate from liquids with different A/Y ratios (i.e. AY-*N*, where *N* is the mol% Y_2O_3 component present) [34, 92, 117, 118]. We concentrated our neutron and x-ray experiments on two glass compositions formed near the metastable eutectic formed between $YAlO_3$ (i.e. the composition of the perovskite-structured crystalline phase in the system) and alumina. A single-phase HDA polyamorphic form of the Y_2O_3–Al_2O_3 glass was obtained consistently at a composition close to the minimum of this eutectic (25% Y_2O_3, or AY-25). That metastable polyamorph was obviously quenched metastably from the HDL supercooled liquid at a rate that allowed it to by-pass the occurrence of the HDL–LDL transition during the quench [53, 54, 64, 92, 117, 119, 120]. However, at the 20% Y_2O_3 (AY-20) composition, two-phase glass samples containing both HDA and LDA components were produced (figure 2). In this case, partial sampling of the HDL–LDL transition occurred during quenching [64, 92, 118, 119]. Some Bragg peaks were always observed in the neutron and x-ray data for such samples, due to the competing partial (usually <5%) recrystallization into a metastable garnet-structured $Y_3Al_5O_{12}$–Al_2O_3 solid solution phase (YAGss) that can be sampled simultaneously with the L–L transition (figure 3).

The amorphous scattering data provide important constraints for beginning to understand the structural differences between the low- and high-density polyamorphs, particularly concerning (a) the nearest-neighbour coordination number around the Al^{3+} and Y^{3+} ions, and (b) the next-nearest-neighbour environments (i.e. Y···Al and Y···Y coordinations). In figure 4(a), we show the radial distribution functions for the two glasses derived from neutron scattering data obtained at SANDALS. We also present results from a combined Fourier transform of the neutron and x-ray scattering data, that permits us to eliminate the O···O correlations from the scattering function [92] (figure 4(b)). The assignment of peaks

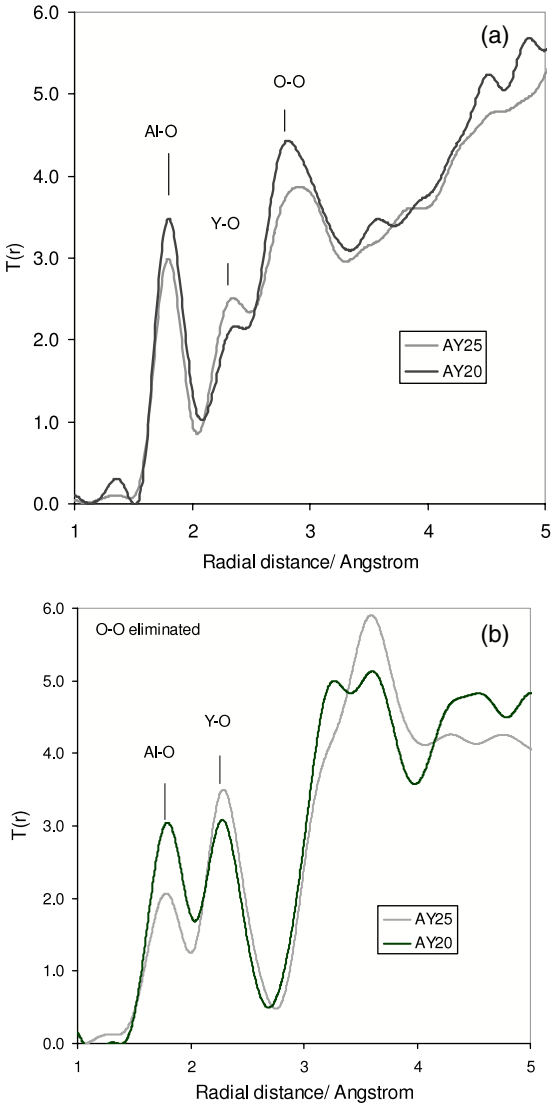

Figure 4. Radial distribution functions for polyamorphic Y_2O_3–Al_2O_3 glasses. (a) Neutron pair correlation functions compared for (i) a single-phase (AY-25: HDA) and (ii) a two-phase (AY-20: HDA + LDA) Y–A glass. The RDFs were obtained by minimum noise Fourier transform of the total $S(Q)$ collected to a maximum $Q \sim 40$ Å^{-1}. The first peak at 1.8 Å corresponds to the Al–O pair correlation and its position indicates a dominantly tetrahedrally coordinated environment around Al^{3+} ions in both samples. The peak at 2.3 Å in the AY-25 glass is due to Y–O correlations. In the AY-20 glass the Y–O correlation contains new contributions at lower and higher r, superimposed on the main O–O peak at 2.8 Å. (b) Pair correlation function for the same two glass samples produced by constructing a difference plot (i.e. $\Delta S(Q)$) using combined neutron and x-ray diffraction data. This procedure eliminates the contribution of O–O correlations to the pair distribution function. Differences in the relative intensities of Al–O and Y–O peaks simply reflect the different Al:Y ratios between the two samples. However, there is a large difference between the two glass structures evidenced by the metal–metal correlations at 3.5–5 Å. In the AY-20 sample the peak at 3.1 Å becomes more prominent (the Y–Al contribution) while the peak at 4.5 Å (Y–Y) increases in intensity. These changes are interpreted as due to differences in the connectivity of Y–O and Al–O coordination polyhedra between HDA and LDA polyamorphs. A detailed analysis of similar data sets has been presented by Wilding *et al* [92].

in the radial distribution functions is mainly based on previous knowledge and experience with crystalline samples, but is also derived from MD simulations carried out on Al_2O_3–Y_2O_3 supercooled liquids at the AY-20 and AY-25 compositions (see below) [91, 92]. It should be noted that differences in the relative intensity of peaks in the radial distribution functions of AY-25 and AY-20 glasses are due to the change in Al_2O_3/Y_2O_3 ratio, as well as to the presence (AY-20) or absence (AY-25) of the LDA component in the glass.

During early investigations of the aluminate glasses, it had been thought that a change in the average Al–O coordination might be primarily responsible for the density difference between HDA and LDA polyamorphs. However, this is not borne out by the experimental results. The Al–O peak is observed for both AY-25 and AY-20 radial distribution functions at 1.8 Å, indicating a predominantly fourfold coordination environment for Al–O in both samples. There was no observable change in peak position, intensity or width of the Al–O correlation between HDA and LDA phases, indicating that the Al^{3+} first-neighbour environments are nearly identical in both samples (figure 4). The mean Al–O coordination number is determined to be 4.16 and 4.28, respectively, for the AY-25 and AY-20 samples. Obviously, no dramatic change occurs in the Al–O coordination that could account for the polyamorphic behaviour. This result was confirmed by ^{27}Al NMR studies, that detected only a small percentage of five- and six-coordinated Al environments in both samples [64, 117]. Likewise, changes in the first-neighbour Y^{3+} coordination behaviour cannot be used to rationalize the polyamorphism phenomenon. The Y–O first-neighbour correlation occurs at 2.3 Å and the coordination number is ∼6.7 for both glasses, smaller than the value for crystalline $Y_3Al_5O_{12}$ or $YAlO_3$ (the Y–O correlation is more clearly seen in figure 4(b), with the O···O contribution removed: see below). ^{89}Y NMR spectra also suggest that the Y–O environment is the same in the two polyamorphs [119].

Our next step was to investigate structural changes among next-nearest-neighbour environments, i.e. within the Al···Al, Al···Y and Y···Y correlations that reflect the metal cation arrangements and clustering in the different glass structures, that might explain the polyamorphism. The neutron scattering function is dominated by contributions from oxygen atoms, meaning that any changes in the medium-range order that are associated with metal–metal interactions in the second coordination shell (∼3–5 Å) are masked by the O–O correlations (figure 4). However, complementary information obtained from high-energy synchrotron x-ray scattering allowed us to remove the oxygen correlations from the pair distribution function analysis, via combined Fourier transformation of the x-ray and neutron scattering data (figure 4) [92]. The Al–O and Y–O first-neighbour pair correlations are now clearly identified, and the effect of the slightly different Al_2O_3/Y_2O_3 ratio is clearly visible in the relative intensities. Large changes in the pair distribution function between the two samples are present at ∼3.5 Å, that results from overlapping Y···Y, Y···Al and Al···Al correlations, and at ∼4.5 Å, that can be traced to differences in the second-nearest-neighbour coordination environments defined by linked polyhedral units in the two glasses. In our previous study, we reported results of a reverse Monte Carlo analysis of the neutron and x-ray scattering data, that allowed us to suggest a preliminary structural model for the differences between the HDA and LDA glassy polyamorphs [92]. In the HDA polyamorph, the Y–O polyhedral clusters appeared to form a discontinuous network of YO_7 with some YO_8 units that are corner shared with AlO_4 tetrahedra. Clustering was also observed within the Al–O framework, instead of the continuously polymerized corner-shared networks usually associated with aluminate glasses [145]. The LDA glass structure appeared to be more homogeneous, in that the Y–O units were more isolated and they shared edges with AlO_4 groups; the abundance of YO_8 units remained the same between the two polyamorphs, but they were mainly corner shared with other Y–O units in the LDA structure [92].

We then extended our structural studies by carrying out polarizable ion MD simulations of Y_2O_3–Al_2O_3 liquids [64, 91, 92]. The simulations allowed us to obtain a more detailed interpretation of the x-ray and neutron scattering data, and to construct a more detailed model for the HDL/HDA and LDL/LDA structures, as well as giving new insights into the L–L phase transition [91, 92].

The potentials used for these simulations were designed to be computationally tractable, allowing calculations to be carried out over long simulation timescales for reasonably large systems, within readily available computing resources. They were based on pair-potential ionic models, augmented with a description of many-body ion polarization effects (i.e. PIMD or AIMD models), using parameters derived from electronic structure calculations [146, 147]. Constant P–T simulations were performed on systems containing 640 ions corresponding to the AY-20 and AY-25 compositions [64, 91, 92]. Similar calculations have also been reported for liquid Al_2O_3 [148], that are relevant to the new x-ray scattering results described here.

It is important to note that the MD simulations cannot access the L–L transition directly. It is a simple matter to carry out simulations for the one-phase liquid existing at high T, well above the L–L transition point, and these calculations can be pursued to low T to well within the metastable supercooled regime. Here, the MD simulations have an advantage over experimental studies in that there is no competing tendency toward metastable crystallization, because crystal nucleation is often heavily suppressed within the simulation box. However, this also means that, because the simulated system is too small to sample such first-order nucleation and growth events, the same holds true for the polyamorphic HDA–LDA transition that should be encountered during cooling. A second problem is that structural relaxation and phase transition nucleation times become exponentially longer as the T is decreased, and these greatly exceed the available simulation timescales as the L–L transition is approached. The best that can be done is to sample the system behaviour in progressively smaller increments as T_c or T_{LL} is approached [64, 91, 92, 96]. However, the structures examined upon quenching are generally those corresponding to the high-density liquid phase that is stable at high T. In our studies, however, we have identified a volume instability occurring within simulated liquids equilibrated close to the L–L phase transition line, that might correspond to sampling the low- and high-density configurations within the one-phase regime (figure 5). Those results allow us to examine the likely structural differences between LDL/LDA and HDL/HDA polyamorphs. We describe the appearance and significance of these volume fluctuations below. However, first we assume that they give information that is complementary to the neutron and x-ray scattering experiments for determining the structural state of HDA and LDA samples.

The simulation models for AY-25 and AY-20 compositions provide an excellent fit with the observed neutron and x-ray scattering spectra (figure 3). They also lead to a much more detailed interpretation of the individual pair correlation functions. Breakdown of the total scattering functions into weighted contributions from the six partial structure factors show that the x-ray scattering is dominated by Y–Y correlations, $S_{YY}(Q)$, as expected (figure 6(a)). Although the mole fraction of the Y^{3+} sub-density is small, its greater number of electrons relative to Al^{3+} and O^{2-} leads to a much larger form factor weighting for those partial structure factors that include Y^{3+}. However, the other partial structure factors also play a significant role in determining the peak positions and shapes over various scattering angle ranges in $F^{xrd}(Q)$. For example, the main peak is shifted to higher Q with respect to that in $S_{YY}(Q)$ by significant contributions occurring from $S_{AlY}(Q)$, $S_{OO}(Q)$ and $S_{AlAl}(Q)$ (figure 6(a)). In addition, the oscillation occurring at larger scattering angles ($\geqslant 5$ Å^{-1}), that we had already anticipated as being important in terms of defining nearest-neighbour ion–ion separations and coordination environments, appears to be less dominated than expected by $S_{YY}(Q)$, which becomes relatively featureless at larger scattering angles, but is rather the combined result of

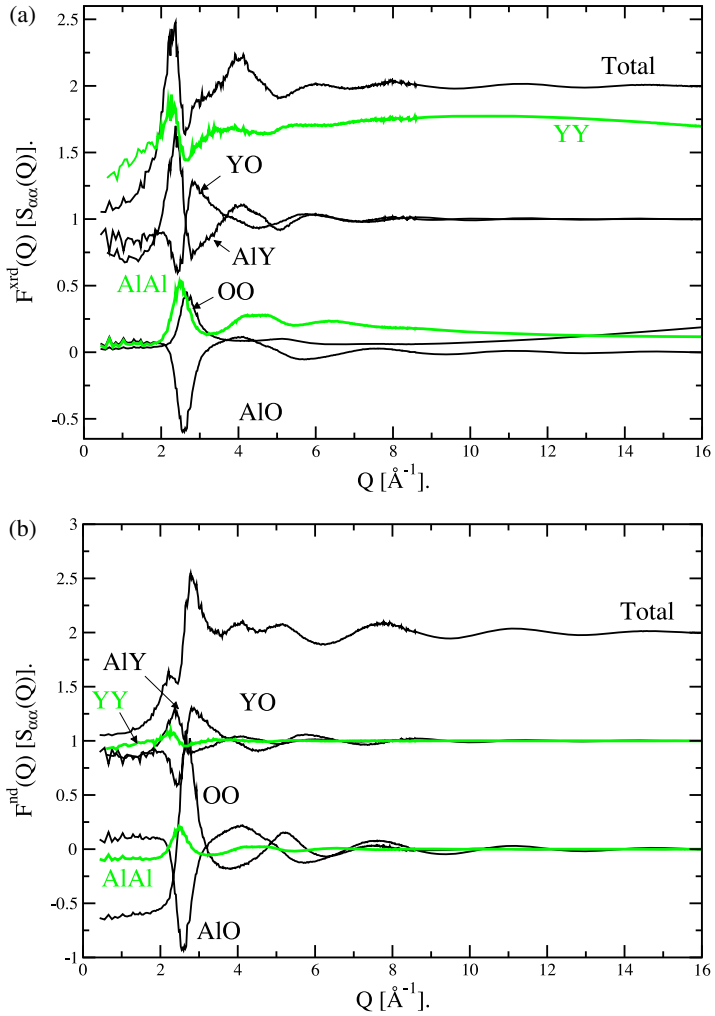

Figure 5. Upper panel: random volume fluctuations observed for an AY-20 simulated liquid following equilibration at 2400 K. Here we show a typical fluctuation of the whole cell volume during a short (0.6 ns) section of the MD simulation at this temperature: such random volume fluctuations occurred during the entire simulation period. We show the high- and low-density excursions that occur at two standard deviations away from the mean liquid volume as light dashed lines. Lower panel: partial pair distribution functions calculated for the low- and high-density extrema using configurations coloured by the cell volume limits shown above. The functions calculated from the high-density configurations are shown as dashed lines, and those from the low-density configurations as solid lines. The like–like functions (O–O, Al–Al and Y–Y partial rdfs) have been shifted relative to each other for clarity.

strong oscillations in the $S_{\mathrm{AlY}}(Q)$, $S_{\mathrm{AlO}}(Q)$, $S_{\mathrm{YO}}(Q)$ and $S_{\mathrm{AlAl}}(Q)$ functions in this region (figure 6(a)). Within the total neutron scattering function (figure 6(b)), the similarity between scattering lengths for the three ions means that the relative weightings of the six partial structure factors are dominated by the mole fraction of each ion type, i.e. by $S_{\mathrm{OO}}(Q)$ contributions. Again, however, the other partial scattering functions also play a crucial role in determining the position and shape of the observed peaks. The main peak in $F^{\mathrm{nd}}(Q)$ is shifted to larger

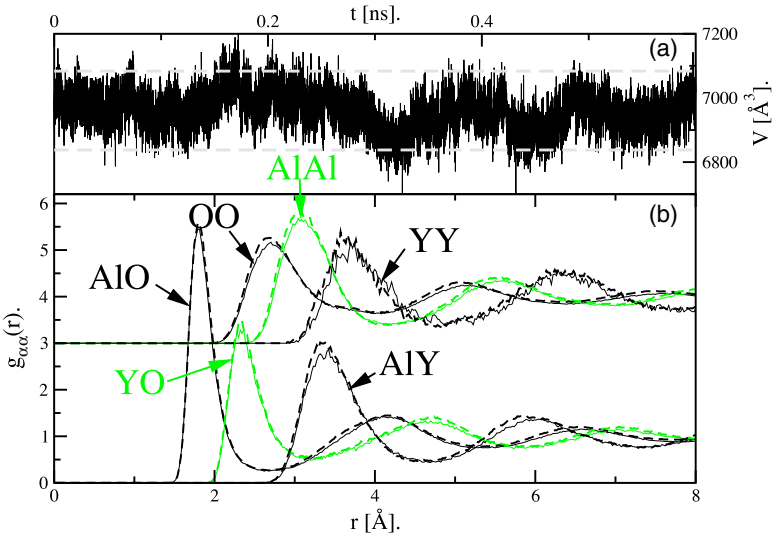

Figure 6. Calculated partial structure factors for (a) total x-ray and (b) neutron scattering functions for AY-20 liquid similated at 2400 K using a polarizable ion model [91, 92]. (a) X-ray scattering. The partial structure factors are shown weighted by the appropriate form factors and are shifted along the *y*-axis, for clarity. The upper (black) lines are the total scattering function obtained by summing the individual partial structure factors in each case.

scattering angle with respect to that of $S_{\mathrm{OO}}(Q)$ via strong contributions from $S_{\mathrm{AlO}}(Q)$ and $S_{\mathrm{YO}}(Q)$. The observed 'shoulder' on the main peak at 2.2 Å^{-1} appears to result mainly from contributions from $S_{\mathrm{AlY}}(Q)$ and $S_{\mathrm{YY}}(Q)$ (figure 6(b)). The region immediately beyond the main peak shows the poorest agreement with experiment. However, in this region, there is near-perfect cancellation of the contributions from the different partial structure factors, so that any slight imperfections in either the experimental data or the simulation model, or the resulting combination of the partials, will be disproportionately magnified into an apparently large discrepancy in $F^{\mathrm{nd}}(Q)$. These combined results illustrate the immense power of not only combining the amorphous scattering results from both neutron and high-energy synchrotron x-ray experiments, but also using MD simulations both to help interpret the data and to carry out a detailed interpretation of the scattering functions.

Performing constant-P MD simulations also allowed us to monitor the system density (i.e. $\rho = 1/V$) as a function of simulation time, during long-timescale runs for systems that were nominally equilibrated, especially as the T was lowered toward the predicted L–L transition. The results of these MD studies have led to new insights into the nature of the density-driven polyamorphic L–L phase transition. Once the system was equilibrated, the MD density was found to fluctuate significantly and randomly during the course of the whole run, remaining at high versus low densities for significant periods of time (figure 5). We interpreted these observations in the following way. For a simple ionic system that yields a liquid with no propensity to undergo density-driven phase separation, the equilibrium volume should simply oscillate about a mean value as a result of instantaneous P fluctuations that are inherent in the simulation cells, and that result from vibrational modes or occasional ionic diffusional displacements. In the present case, however, this did not occur. Our interpretation of the behaviour was that the system had sampled high- and low-density configurations present within the one-phase liquid above T_{LL}, and that these dynamically interchanging nanoscale domains

would evolve into the HDL and LDL phases observed to appear below the macroscopic phase transition point. Our simulations were performed at sufficiently high T to allow the ions to effectively sample phase space during the available simulation timescales. However, even though the system lies above T_{LL}, it can still sample configurations with local ion geometries that are consistent with the high- and low-density two-phase region; the system energy is simply greater than the barrier that must separate the HDL/HDA and LDL/LDA configurational 'basins'. This observation provides a strategy to compare the likely structural properties of HDA/LDA polyamorphs and investigate the nature of the density-driven L–L transition directly, even though the simulation T must be kept significantly above T_c in order to achieve MD system equilibration within a reasonable time.

An atomistic origin of the structural differences associated with the density fluctuations and the HDL–LDL transition can be understood by reference to the partial radial distribution functions (prdfs) calculated from those low- and high-density configurations that occurred within $\pm 2\sigma$ from the mean density (figure 5). The (Y, Al)–O prdfs show only small differences between the high- and low-density limits, indicating that the cations are in similar coordination environments. This is consistent with the conclusion from the experimental results described above. However, significant differences are seen in the Y $\cdots$ Y structural correlations. In the low-density limit the first peak in the prdf is shifted to higher r with respect to that in the high-density limit, and a shoulder is present at low r. Analysis of the cation–cation coordination environments shows that, on average, the Y^{3+} cations in the low-density limit are coordinated to a greater number of Y atoms (i.e. via oxide bridges) than is the case in the high-density-limit liquid. Overall, the Y^{3+} sub-density is more highly clustered in the low-density limit, but it is more uniformly distributed in the HDA regime. This interpretation is consistent with the experimental observation that the LDL phase has lower configurational entropy than the HDL/HDA polyamorph [53, 54, 117]. The configurations calculated from the low- and high-density regions in the Y_2O_3–Al_2O_3 liquids are comparable with those obtained by RMC modelling of the experimental x-ray and neutron scattering data for the AY-20 and AY-25 glass compositions (figures 7 and 8).

The MD prediction of dynamic density fluctuations occurring on a nanoscale within supercooled Al_2O_3–Y_2O_3 liquids upon approach to the density-driven L–L phase transitions has now been confirmed by recent small-angle x-ray scattering (SAXS) complemented by 'wide-angle' (WAXS) amorphous diffraction experiments, using aerodynamic levitation techniques to obtain a containerless environment at beamline 6.2 of the Synchrotron Radiation Source (SRS), Daresbury, UK [149] (figures 9 and 10). Similar WAXS data for Al_2O_3–Y_2O_3 liquid samples at high T have been obtained at station 11 ID-C at the APS [83, 150, 151]. Containerless levitation techniques have been applied to *in situ* studies of Ge and Si liquids using x-ray scattering or absorption and EXAFS studies [59, 80, 84, 152, 153]; the results of this work are described below. They have now been implemented for *in situ* structural studies of refractory oxide liquids using synchrotron x-ray and neutron scattering techniques [61, 154–163]. Containerless levitation methods have previously been combined with NMR spectroscopy to carry out *in situ* structural studies of aluminate liquids at high T, and also to synthesize Y_2O_3–Al_2O_3 glasses using fibre-pulling techniques [82, 164–169].

The samples studied by SAXS at Daresbury SRS 6.2 were levitated using a specially designed containerless levitator constructed at the University of Wales, Aberystwyth. Al_2O_3 and Y_2O_3–Al_2O_3 liquids were first formed by heating polycrystalline materials to above the stable melting T using a CO_2 laser. Once the levitated liquid droplets had stabilized, the liquids were cooled by gradually reducing the laser power and *in situ* x-ray scattering data were collected. Temperature was constantly monitored by pyrometry and video images of the levitated droplets were obtained in real time. Density fluctuations in liquids can be detected

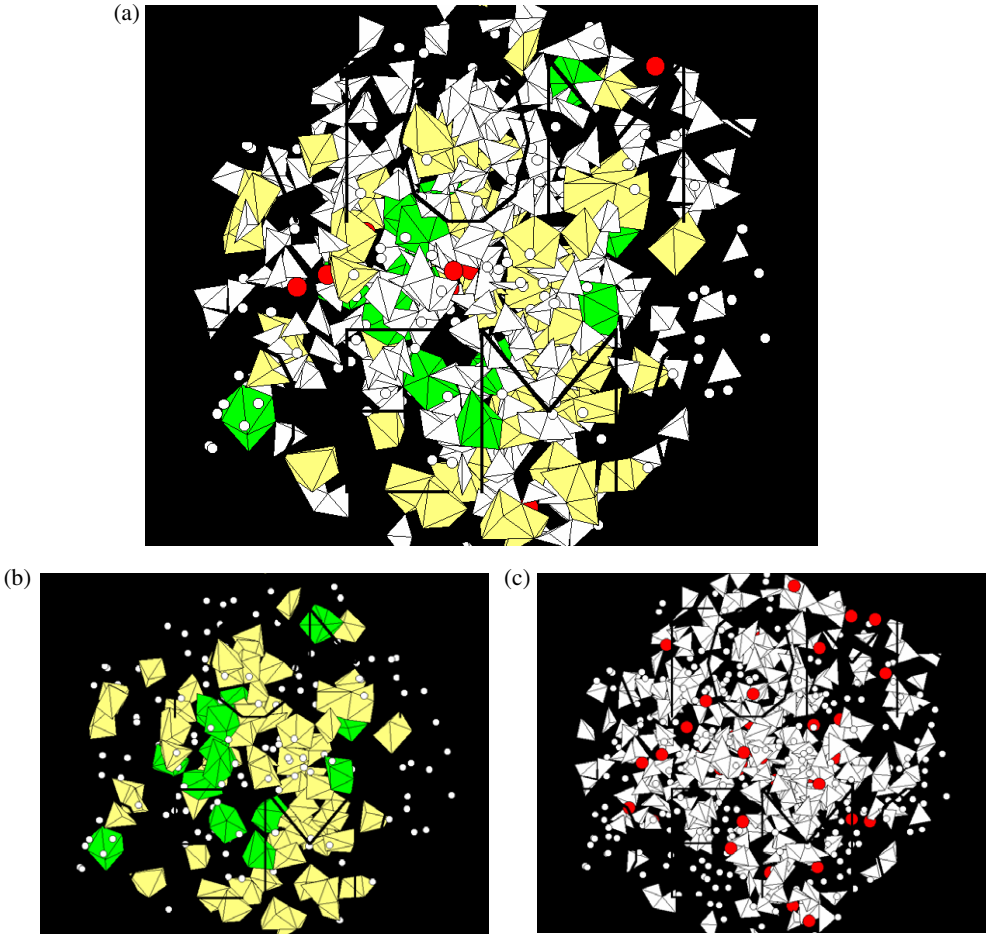

Figure 7. Reverse Monte Carlo fit to diffraction data for AY-25 glass. (a) This rendering shows the four-coordinated Al–O units (white) along with the seven-coordinated (yellow) and eight-coordinated (green) Y–O polyhedra (A). The aluminate contribution is eliminated from (b) and Y–O units are not shown in (c).

from the minimum in small-angle scattering at the foot of the structure factor [47]. SAXS rises as Q decreases further, the slope and magnitude for single-phase liquids decreasing with decreasing temperature. This is illustrated for levitated liquid Al_2O_3 and Y_2O_3–Al_2O_3 liquids in figure 9, where the minimum occurs at around 0.03 $Å^{-1}$: considerably lower than reported previously for molten silica, for example [47]. The size of density fluctuations in simple liquids generally falls linearly with temperature: the decrease between 1848 and 2423 K is shown for molten alumina in figure 9(b). In contrast, the opposite behaviour occurs for levitated AY-20 liquid when the temperature is lowered, with the SAXS intensity, $I(Q)$, increasing sharply around 1973 K (figure 9(a)). This increase in $I(Q)$ measured *in situ* for supercooled AY-20 [149] heralds the liquid–liquid transition and is consistent with the onset of unmixing of HDL and LDL polyamorphs at the nanoscale. Indeed, $I(Q)$ should eventually pass through a maximum at the 50/50 mixture for a simple binary phase transition [47]. Interestingly, when temperature gradients are present in levitated liquid AY-20, macroscopic segregation of LDL

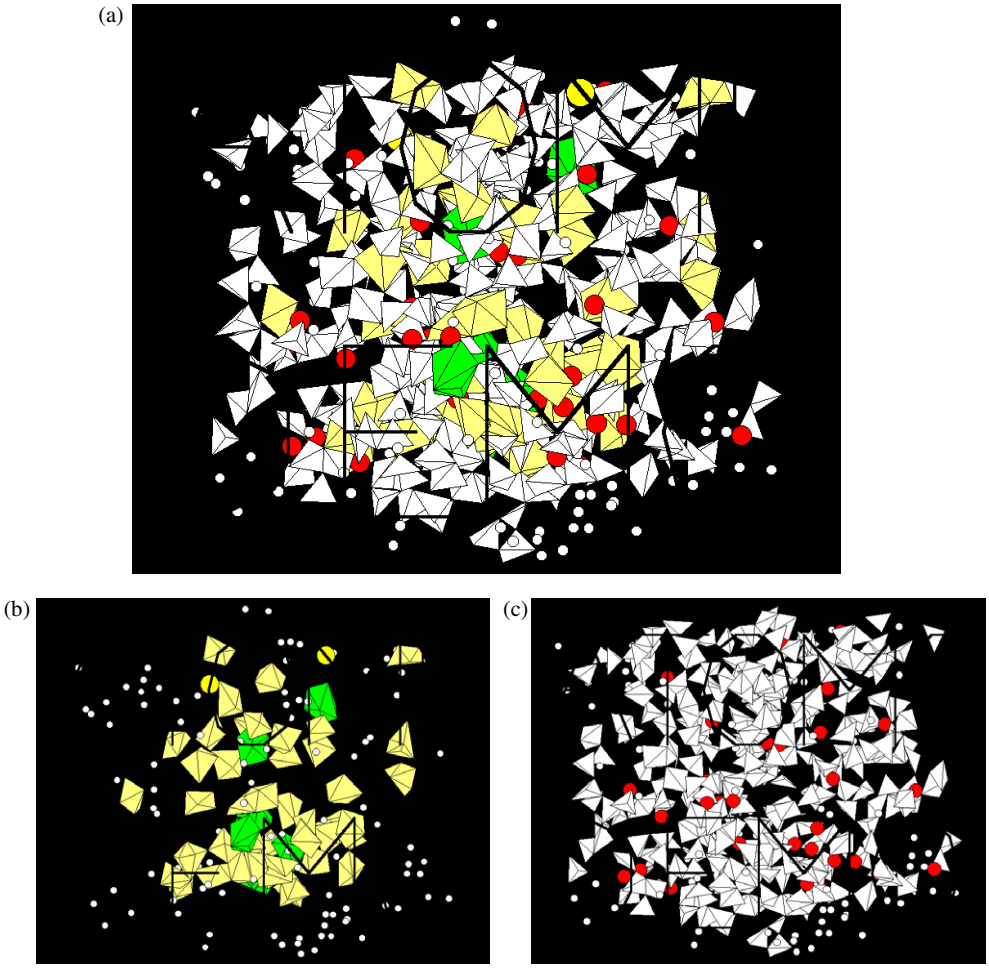

Figure 8. Reverse Monte Carlo fit to diffraction data for AY-20 glass. The same schemes are used to describe Al–O and Y–O polyhedra (A) as in figure 7. This model constitutes an 'averaged' LDA–HDA mixture.

from HDL phases has been observed [149]. SAXS data in figure 9 for liquid alumina and liquid AY-20 are plotted as $\log I(Q)$ versus Q^2 and display linear regions. Using the Guinier law, the sizes of scattering domains can be analysed from $d(\log I(Q))/\mathrm{d}(Q^2)$ [47] and, for single-phase Al_2O_3 and Y_2O_3–Al_2O_3 supercooled liquids, have diameters of 200 Å [149]. Both are extremely fragile and compressible liquids compared to silica, where scattering domains are about a decade smaller in size [47]. As T_{LL} is approached in supercooled AY-20, scattering domains increase to 270 Å in diameter, consistent with the nanoscale incipient segregation of LDL from HDL liquids detected in the MD simulations at the much higher temperatures illustrated in figure 5.

The changes in the SAXS signal for supercooled AY-20 in figure 9 are also mirrored by changes in the x-ray scattering at large angles (WAXS), which can be measured simultaneously using combined SAXS–WAXS detector geometry [149]. These changes in WAXS are shown in figure 10, where the difference between the stable and supercooled liquid structure factors

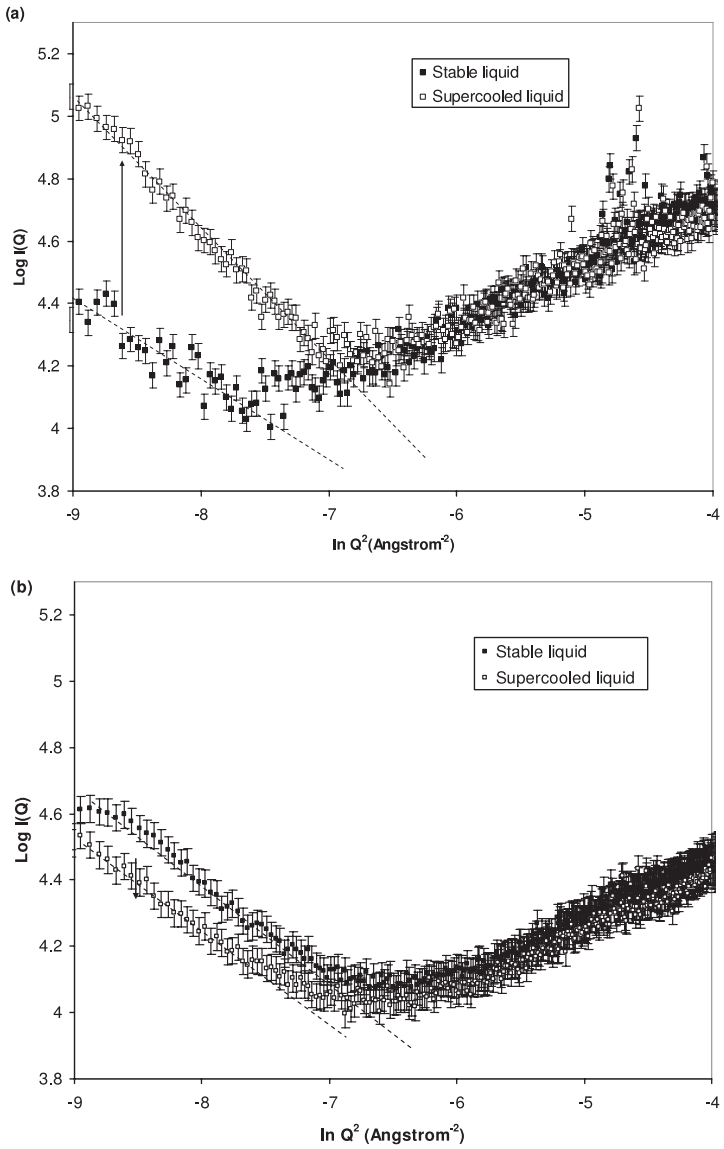

Figure 9. (a) Small-angle x-ray scattering (SAXS) data, plotted as $I(Q)$ versus Q^2, collected at station 6.2, at the Synchrotron Radiation Source, Daresbury, for levitated AY-20 (20% Y_2O_3) aluminate liquid (a) and for pure alumina (b) [149]. In both cases the minimum between the scattering at the smallest angles and the foot of the structure factor, $S(Q)$, occurs in the vicinity of $Q \sim 0.03$ Å^{-1}, shifting to lower Q with increasing Guinier slope. The two liquids behave quite differently in the supercooled regime. For AY-20 there is an *increase* in the $I(Q)$ at around 1848 K as the temperature is lowered (open symbols), compared with the stable liquid at 2423 K (closed symbols). This is shown by the arrow in the inset for (a). SAXS data collected for pure Al_2O_3 liquid at similar temperatures (b) show a *decrease* in intensity (shown by the arrow in (b)), as is expected for 'normal' supercooled liquids with falling temperature.

$S(Q)$ is plotted. $\Delta S(Q)$ reveals peaks at 2.2 and 4.13 Å^{-1}, features which we have already associated with ion–ion pair correlations from the MD simulations of $F^{\mathrm{xrd}}(Q)$ and $F^{\mathrm{nd}}(Q)$

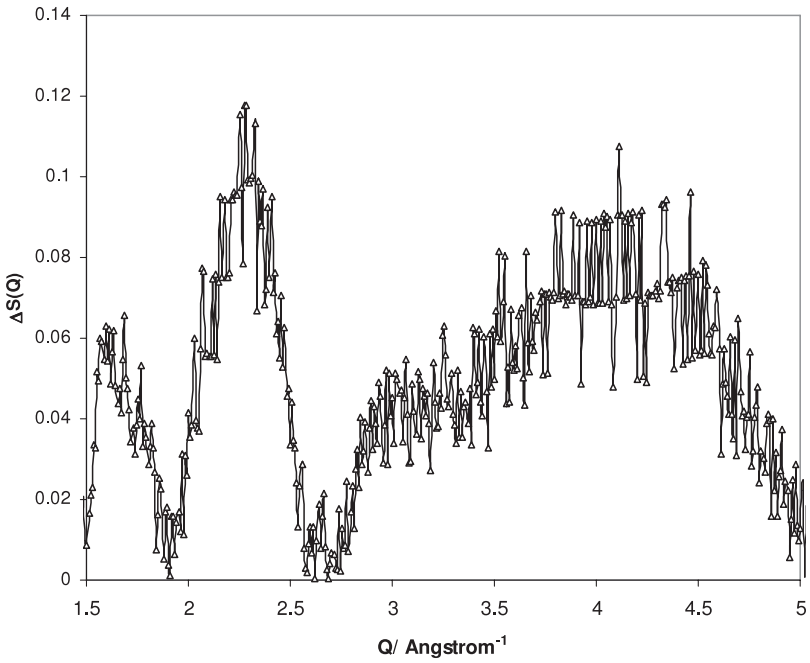

Figure 10. Wide-angle (WAXS) data collected simultaneously with the SAXS data for the AY-20 liquid at SRS 6.2 [149]. Differences in the diffraction patterns between the high-T (2423 K) and supercooled (1848 K) liquids relate to the structural changes in polyhedral configurations that accompany the HDL–LDL transition.

(figure 6). Features at similar Q values have also been seen in high-energy x-ray diffraction data obtained at APS for AY-20 glass and for levitated liquid $Y_3Al_5O_{12}$ samples [92, 150]. In particular, the peaks at 2.2 and 4.13 Å are also found in $S_{Y-Al}(Q)$ differences between HDA and LDA recovered Y–A glasses obtained from RMC fits to combined neutron and x-ray diffraction data [78, 104].

To summarize, for the AY-20 liquid sample that is known to sample the L–L phase transition during supercooling from our previous quench experiments [34, 92, 117, 118], there is a large change in the $S(Q)$ during cooling between 1973 and 1848 K. This corresponds to an increase in the magnitude of the WAXS peak at 2.2 $Å^{-1}$ and the growth of a shoulder at ∼3.5–4 $Å^{-1}$, over the same T range for which a maximum occurs in the SAXS signal (figure 10). The SAXS data for the levitated AY-20 supercooled liquid indicate that structural/density fluctuations appear in the liquid on a length scale of 7–13 Å as T is decreased toward the onset of the L–L phase transition (figure 9). This observation is consistent with the random density excursions recorded within the MD simulated liquid—albeit at temperatures above T_{LL}. We conclude that the liquid is sampling dynamic nanoscale density fluctuations within the homogeneous liquid, just above the onset of the macroscopic thermodynamic density-, entropy-driven L–L phase transition. Similar fluctuations at the sub-micron scale in polyamorphic liquids above T_c or T_{LL} have been observed using phase contrast microscopy in the case of triphenyl phosphite [50], and analogous nanoscale dynamic heterogeneities have been invoked to interpret the changes in electrical conductivity and other physical properties observed in the stable liquid phases of elemental systems such as S, P, Te, I or Se at high-P, T conditions [45, 113].

3. Polyamorphism in solid amorphous Si and Ge and a liquid–liquid phase transition in the supercooled state

X-ray and neutron scattering combined with XAS studies of a-Si and a-Ge and their corresponding liquids have contributed substantially to our understanding of the occurrence of polyamorphism in these technologically important systems. The crystalline forms of these materials at ambient P have a tetrahedrally bonded diamond structure. The corresponding amorphous solids that are generally produced by chemical or physical vapour deposition methods likewise provide important semiconducting materials [116]. The crystals undergo extensive polymorphism at high P, leading to metallic phases in which the Si or Ge atoms are present in octahedral or even higher coordination environments [11]. The liquid formed by melting the semiconductor crystals at low P also has metallic conductivity, and it possesses a higher density than the crystal phase, so that the melting slope (dT_m/dP) recorded at $P > 1$ atm is negative. The melt density is also greater than that of the solid amorphous semiconducting form. However, once the crystal has transformed to the β-Sn structured phase or other high-pressure crystalline forms the melting curve obtains a normal positive slope (figure 11). It has long been surmised that some unusual type of transformation must be present to link the low-density amorphous semiconductor with the metallic liquid, not only for Si and Ge, but also for other amorphous semiconductor systems [170].

A two-state model was applied by Aptekar to understand the unusual melting phenomena observed in these systems; related thermodynamic models were developed in later work [1, 26–28, 30, 55, 75, 96]. The volume contribution of the low-density component was modelled on the sp^3-bonded crystalline semiconductors, whereas the high-density domains were taken to resemble the six-coordinated species found in the β-Sn structured polymorphs. Such thermodynamic models predict a melting curve maximum occurring at negative pressure in the tensile regime ($P \sim -1$ GPa), close to the predicted tensile limit for the bulk liquids [1, 24, 27, 28, 55] (figure 11). Such a regime is experimentally achievable: lattice strains corresponding to tensile stresses of the order of $P \sim -1$ to -3 GPa have been recorded for crystalline Si in semiconductor structures, so these negative pressures may be accessible for future experimental studies [24]. The two-state models predict a critical point for supercooled liquid silicon (l-Si) occurring at $P_c \sim -1$ GPa and $T_c \sim 1100$ K, below which an LDL–HDL phase transition is expected to occur (figure 11). Similar results are expected to occur for supercooled l-Ge [1, 55, 57, 84].

The first experimental evidence for an unusual transition linking the tetrahedrally bonded amorphous semiconductor (i.e. the LDA polyamorph) and the supercooled metallic liquid state (HDL) was obtained during short-timescale measurements of the 'melting' T, along with the heat capacity and other physical properties, of a-Si layers during flash laser heating techniques [52, 171, 172]. The transition between LDA and HDL was observed at ∼200 K below the melting point ($T_m = 1480$ K), in the supercooled liquid regime. It is important to note that, at this point, several important processes remain to be clarified. If the observed 'metastable melting' transition in a-Si (and predicted for a-Ge) were in fact related to an underlying density-driven L–L phase transition, the observed physical property changes and calorimetric data could incorporate the glass transitions of both LDA–LDL and HDA–HDL materials (T_g^L, T_g^H), as well as the first-order LDL–HDL transition (or its projections on to the non-ergodic HDA and LDA states), and any superheating or undercooling effects towards the low- and high-density spinodal lines. All of these effects are expected to be strongly rate dependent. These questions are still not yet fully resolved, and they represent challenges for future experimental and theoretical studies of polyamorphism within the amorphous semiconductors.

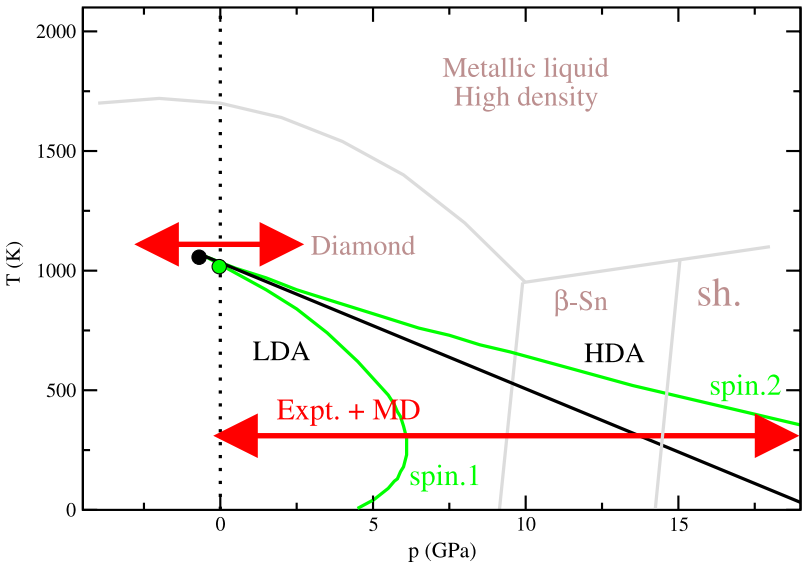

Figure 11. A P–T phase diagram for silicon up to $P \sim 17$ GPa, showing the initial negative melting slope up to the triple point at the diamond (Si-I) to β-Sn (Si-II) boundary. The melting line is continued into the metastable negative pressure regime to highlight the likely occurrence of a melting curve maximum under tensile stresses placed on the liquid–crystal relations. The melting curve at low pressure is constructed from MD simulations and thermodynamic models, constrained by experimental data [1, 24, 28, 55, 96]. The maximum in the melting curve and the initial negative melting slope at $P > 1$ atm are rationalized using a two-state model as described in the text. This model predicts the occurrence of a density-driven liquid–liquid phase transition (i.e. between HDL/HDA and LDL/LDA polyamorphs) below a critical $T_c = 1060$ K at $P \sim -1$ GPa. The L–L transition has a negative Clapeyron slope, and it is expected to cross the $T = 300$ K axis at $P \sim 13$ GPa, ignoring effects associated with the glass transformation in LDA or HDA phases. Upper and lower spinodals are also associated with the LDA–HDA transition: these are shown as green lines in the figure. Our experimental studies on a-Si have been concerned with pressurization at ambient T, represented by the lower red arrow in the diagram. We have also used MD simulations to probe the a-Si behaviour under these conditions, using a modified Stillinger–Weber potential function to reproduce the starting glass structure at ambient conditions. We also carried out MD simulations of the supercooled liquid behaviour during approach to the onset of T_c and T_{LL}, over a P range indicated by the upper red arrow.

Ge K-edge XAS and EXAFS spectra of liquid Ge were first studied *in situ* as a function of cooling using containerless levitation techniques into the deeply undercooled regime, down to 950 K (∼300 K below T_m) [84]. The first-shell distances increased from 1.83 Å in the high-T liquid at 1610 K to 2.30 Å in the supercooled liquid at 950 K, indicating a gradual lengthening of the Ge–Ge average bond length and possibly suggesting a superposition of six- and four-coordinated states. However, the XAS spectra and the EXAFS oscillations remained consistent with a predominantly high-coordinated liquid structure throughout the T range studied [84]. Interestingly, however, it was observed that rapid recrystallization of the sample occurred into the diamond-structured phase when the sample was cooled to just below 950 K. That temperature corresponds closely to the HDL–LDL phase transition boundary (or its associated spinodal limits) predicted using the two-state model for a-Ge [1, 55]. It is possible that the inherent density fluctuations developed within the supercooled liquid during close approach to the predicted L–L transition line caused sampling of the low-density crystalline states within the potential energy hypersurface, and rapid irreversible crystallization ensued. A similar study

was recently carried out for high-T and supercooled l-Si via high-energy x-ray scattering using containerless levitation techniques implemented at the APS [80]. The high-T liquid above the stable liquidus had a coordination number (CN) $\sim$ 6.5–7.0, and the results indicated a gradual decrease to CN $<$ 5 for the deeply undercooled liquids [80, 152, 173]. During cooling, rapid crystallization into the diamond-structured phase occurred, as observed for l-Ge. A similar result was found by Jakse *et al*, who managed to extend the experimental synchrotron x-ray $S(Q)$ measurements down to 1458 K (i.e. 230 K below T_m) [153]. The effects of sampling such low- versus high-density states in the liquid has been studied using both empirical and *ab initio* derived MD simulations [28, 153, 174]. These observations have been suggested to provide strong evidence for a density-, entropy-driven L–L phase transition occurring in supercooled liquid Si and Ge, as predicted by the Rapoport/Aptekar two-state model. Very recently, the high-density metallic liquid form has been vitrified, by rapid cooling in a laser-heated diamond anvil cell experiment [175]. This work correlates with the polyamorphism recently observed in a multicomponent metallic glass, $Ce_{55}Al_{45}$ [176].

An alternative strategy for studying the polyamorphism in a-Si and a-Ge is to investigate the transformation behaviour of the solid amorphous materials at high P and at ambient to low T. The first experimental evidence for a semiconductor–metal transition occurring within a-Si was provided by Minomura, from electrical conductivity measurements carried out at high P in a large-volume press [177]. It was observed that at $P\sim$10 GPa the resistance dropped by $\sim$5 orders of magnitude. Upon decompression to below $P \sim$ 2–4 GPa, the conductivity of the sample returned to its original value. X-ray examination following decompression to ambient conditions showed that the sample was fully amorphous. It was suggested that a structural or phase transformation had occurred in the amorphous state at high P, between semiconducting and metallic varieties of the amorphous solid [178]. The disadvantage of these experiments was that the sample could not be examined *in situ*, so that any metastable structural or phase transformations including crystallization or re-amorphization could not be observed, and their possible contributions to the electrical behaviour would not be detected. In a later study of a-Si and a-Ge in a large-volume apparatus using synchrotron radiation to penetrate the sample assembly and record x-ray diffraction patterns *in situ* at high pressure, it was observed that the amorphous semiconductors crystallized (at least partially) into their metallic β-Sn structured polymorphs above P = 8–10 GPa, and that the crystalline high-pressure phases subsequently re-amorphized into the semiconducting amorphous state during decompression [179]. It was thus concluded that the resistance change observed in the earlier studies was *not* due to a transformation within the amorphous material, but instead to pressure-induced recrystallization, followed by re-amorphization during recovery of the sample to ambient conditions.

Pressure-induced structural amorphous transformations have also been investigated by amorphous x-ray diffraction experiments carried out in the diamond anvil cell (DAC) [76]. a-Ge and a-Ge:H samples were studied up to 10 GPa using laboratory-based x-ray scattering. At ambient P, first and second amorphous diffraction peaks (FDP, SDP) in $S(Q)$ were observed at 2.0 and 3.5 $Å^{-1}$. Upon pressurization, the SDP remained essentially unchanged in position, but the FDP moved to larger Q values and its width decreased [76]. Above 6.2 GPa, Bragg peaks due to crystallization to the β-Sn structured phase were present in the diffraction pattern. Some crystalline material was also found to be present in the samples recovered to ambient conditions. However, the existence of a possible polyamorphic transition between LDA and HDA phases could not be determined.

In parallel studies of the polyamorphism phenomena in H_2O, that is also a reluctant glass-former like Si and Ge, it has proved critically important to first form the HDA polyamorph via a solid-state PIA process at low T [35, 39, 71, 104]. The usual diamond-structured forms of Si and Ge that are stable at ambient conditions do not readily undergo PIA; instead, rapid

transformation into high-density crystalline phases occurs. However, during a high-P study of a nanocrystalline 'porous silicon' phase (π-Si), we first observed PIA to occur, that was characterized using laboratory Raman spectroscopy and energy-dispersive synchrotron x-ray diffraction in the DAC [27]. The a-Si material formed at high P via PIA was found to be quite different from that of the usual LDA form of a-Si prepared at ambient conditions, and we concluded that an HDA polyamorph of a-Si had been formed. During decompression, the HDA a-Si form back-transformed into the LDA polyamorph, below $P \sim 5$ GPa [27]. These results provided important support for the LDA–HDA transition model.

In our work, we first conducted an *in situ* high-P study of the polyamorphism in a-Si using Raman spectroscopy combined with electrical conductivity measurements in the DAC at $T = 300$ K [28] (figure 12). The HDA–LDA polyamorphic transition was observed as a dramatic change in the Raman-active vibrational density of states (VDOS), occurring at $P =$ 14–15 GPa during compression. The characteristic Si–Si stretching and deformation modes of the tetrahedrally coordinated amorphous network were replaced by features concentrated in the lower frequency range, consistent with transformation to an amorphous structure with higher average coordination number. That interpretation was supported by the results of MD simulations [28]. Electrical conductivity experiments showed a large resistance drop during the LDA–HDA transformation (figure 12). The polyamorphic transformation was found to be reversible upon pressure release, with a large hysteresis. Both the LDA–HDA and subsequent HDA–LDA back-transformations occurred at approximately the pressures of the high- and low-density spinodals predicted by the two-state model for liquid Si, that results from the predicted density-driven L–L transition in the supercooled state.

We continued our studies of polyamorphism in a-Si using angle-dispersive x-ray scattering carried out in the DAC at high pressure at the ESRF synchrotron station ID-15 [75]. That experimental study was combined with MD simulations in order to help interpret the observed changes in $S(Q)$ as a function of P and obtain the derived radial distribution functions, and also to correlate these with the structural changes expected to occur across the polyamorphic transformation (figure 14). In figure 13, we show the static structure factor for a-Si obtained during compression and decompression. The amorphous $S(Q)$ at ambient P is dominated by two features; a first diffraction peak (FDP) at 2.18 Å^{-1}, and a second peak (SDP) at 3.63 Å^{-1}. At low pressure the FDP is less intense than the SDP, in agreement with previous experimental studies at ambient pressure and MD simulation results [180–182]. The FDP is associated with spatial correlations between neighbouring Si atoms, and also with the sample density. As the pressure is increased to ~13 GPa there is a slight change in the position of the FDP (from 2.18 to 2.23 Å^{-1}), consistent with the expected densification of the tetrahedral LDA a-Si structure upon compression. The relative intensity of the FDP compared with the SDP remains approximately constant throughout this pressure range (figure 13). Above 13.5 GPa, a dramatic change occurs in the $S(Q)$ function, that affects the relative intensities of the two peaks. The FDP abruptly becomes more intense than the SDP, and it shifts abruptly to larger Q (2.48 Å^{-1}). These changes agree with those predicted by MD simulations [75] (figure 14). Within the MD-simulated $S(Q)$, the FDP shifts between 2.06–2.19 Å^{-1} but there is no change in the relative intensities of the first two peaks during the early compression range. However, above $P > 11$ GPa there is a rapid reversal in the relative intensities of the FDP and SDP, and the FDP moves to 2.38 Å^{-1}.

In order to derive useful structural information concerning the polyamorphic transformation, it is necessary to transform the $S(Q)$ data into a radial or pair distribution function (e.g. $g(r)$). This posed a problem for the data analysis within the experimental study, because of the finite Q range that could be studied in the DAC within the experimental

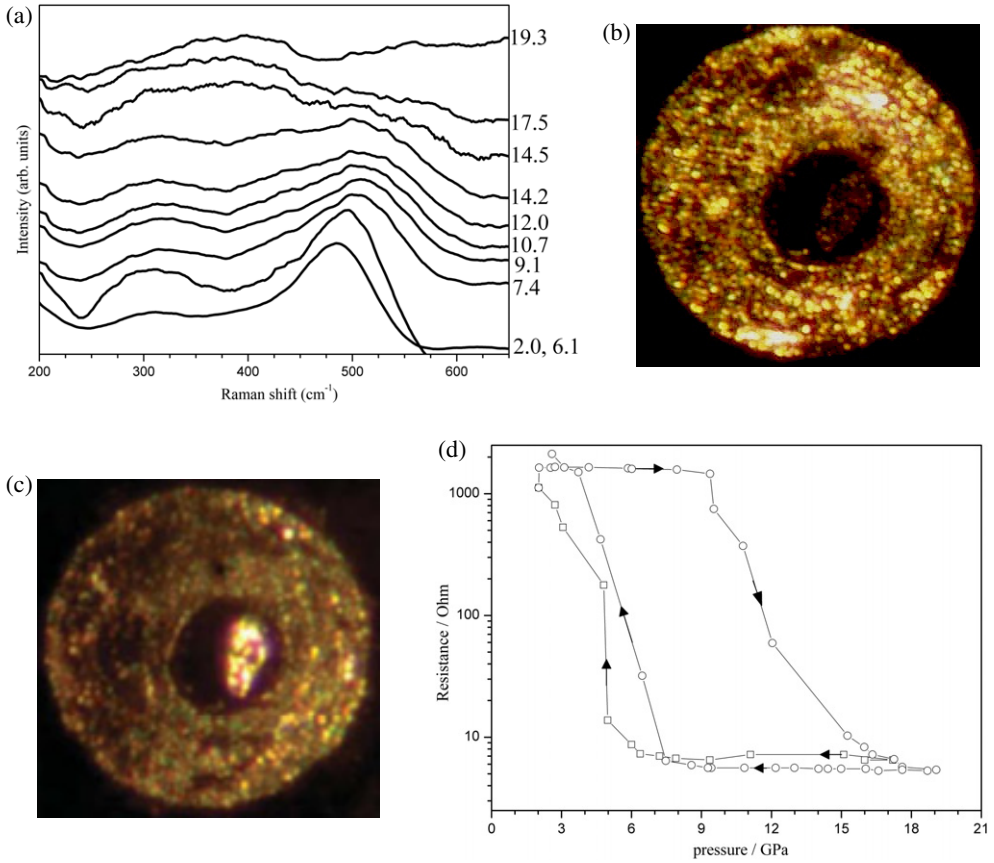

Figure 12. Evidence for a polyamorphic transition occurring in amorphous silicon at high pressure. (a) Raman spectra of a-Si during compression, showing the occurrence of a density-driven amorphous–amorphous transition between the low-density tetrahedrally coordinated polyamorph (LDA) and a new high-density amorphous form (HDA) at $P = 14$–16 GPa during compression. The LDA phase re-appears below 9 GPa during decompression [28]. (b), (c) Optical micrographs obtained for the sample just below and above the polyamorphic transition during compression. The HDA polyamorph is much brighter in reflected light than the LDA form. (d) Electrical conductivity measurements of a-Si during compression and decompression. The HDA polyamorph has substantially lower resistivity, corresponding to metallic behaviour. There is a large hysteresis between compression and decompression runs, as expected for a polyamorphic transition that has quasi-first-order character.

geometry (i.e. up to $Q_{\max} \sim 11$–12 Å, using 52 keV incident x-rays). A 'raw' transform of the experimental data resulted in unphysical oscillations appearing in the $g(r)$ function because of Fourier transform windowing effects (figure 14) [75]. During this first series of experiments, our experimental data set also contained Bragg peaks that appeared due to partial recrystallization of the sample during compression in the highly metastable regime, that had to be removed before analysis of the amorphous $S(Q)$ (figure 13). This issue is discussed further below, and new data are presented here that overcome this problem. However, carrying out MD simulations simultaneously with the experimental study allowed us to usefully interpret the experimentally derived $S(Q)$ and $g(r)$ functions [75], and also to propose structural models for the LDA and HDA polyamorphs (figure 15).

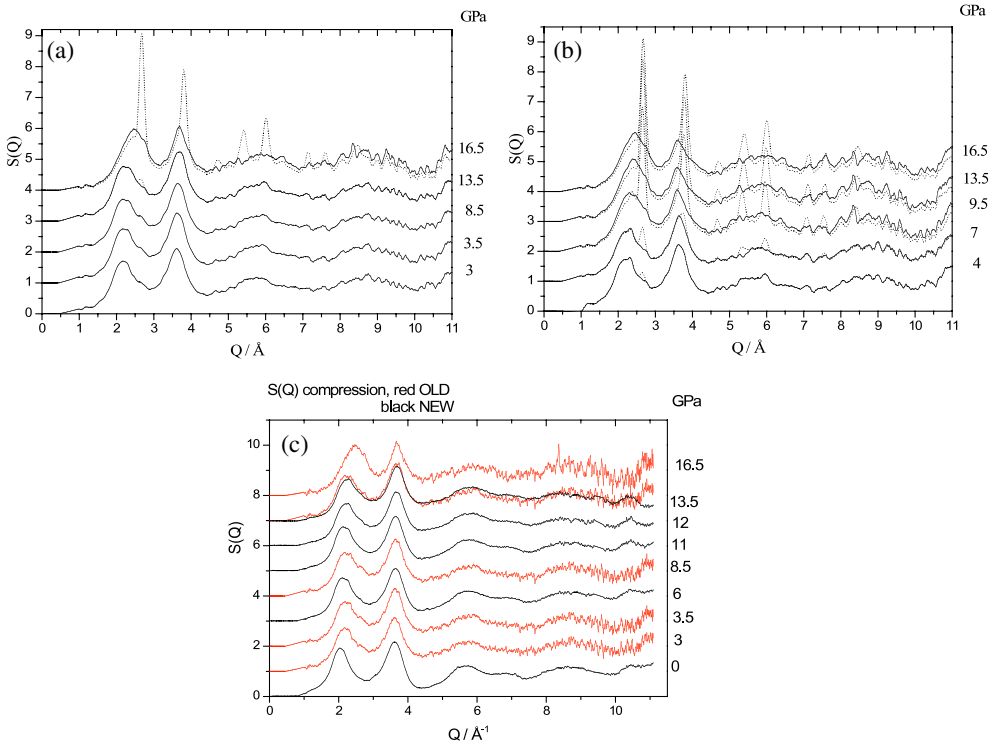

Figure 13. Synchrotron angle-dispersive x-ray diffraction data obtained for a-Si during room-T compression in the DAC. (a) Data obtained at ESRF ID-15A using a $\lambda = 0.238\,431$ Å (52 keV) incident beam that was focused/collimated to 100 μm $\times$ 100 μm, i.e. incorporating a signal from the entire sample chamber [75]. The data set contains Bragg peaks that appear in the $S(Q)$ spectra due to metastable crystallization of the β-Sn structured phase (out of its stability field) at various points within the sample at $P > 13.5$ GPa. (b) During decompression, the Bragg peaks remain down to $P \sim 4$ GPa, at which point the β-Sn (Si-II) crystalline phase re-amorphizes into the LDA polyamorph [75, 179]. For both compression and decompression data sets, the β-Sn (Si-II) Bragg crystalline peaks were removed by hand before analysis of the amorphous scattering. (b) The raw x-ray scattering data obtained using 52 keV x-rays were treated to remove the background signal and Compton and coherent scattering contributions to obtain $S(Q)$ for the sample [75]. (c) Our latest $S(Q)$ results obtained for a-Si at high pressures in the DAC using the high spatial resolution at ID-27 to observe amorphous scattering free from crystalline contributions (see text and figure 15 below), compared with the data obtained from ID-15A results, with Bragg peaks removed.

Our simulations of liquid Si were carried out using a Stillinger–Weber (SW) effectively many-body atomistic potential [75, 183]. Constant temperature and pressure conditions (NPT ensemble) were imposed using Nosé–Hoover thermostats and barostats [184–186]. High-pressure runs of ∼310 ns were performed at 300 K with the pressure ramped by 1 GPa every 10 ns. The initial (zero-pressure) amorphous configuration was obtained using a slightly modified version of the SW potential [75, 187, 188]. Rapid cooling from the melt employing the original potential function results in an over-coordinated, higher-density, amorphous structure, commonly referred to as 'SW glass' [187, 188]. Weighting of the SW three-body term was thus increased during cooling from the melt to enhance the degree of tetrahedral order with respect to the liquid structure [187, 188]. This procedure results in an amorphous structure that contains ∼5.0% three-coordinated and ∼3.2% five-coordinated species. The experimentally determined density of annealed amorphous silicon is ∼1.8% lower than that of Si-I due to the presence of

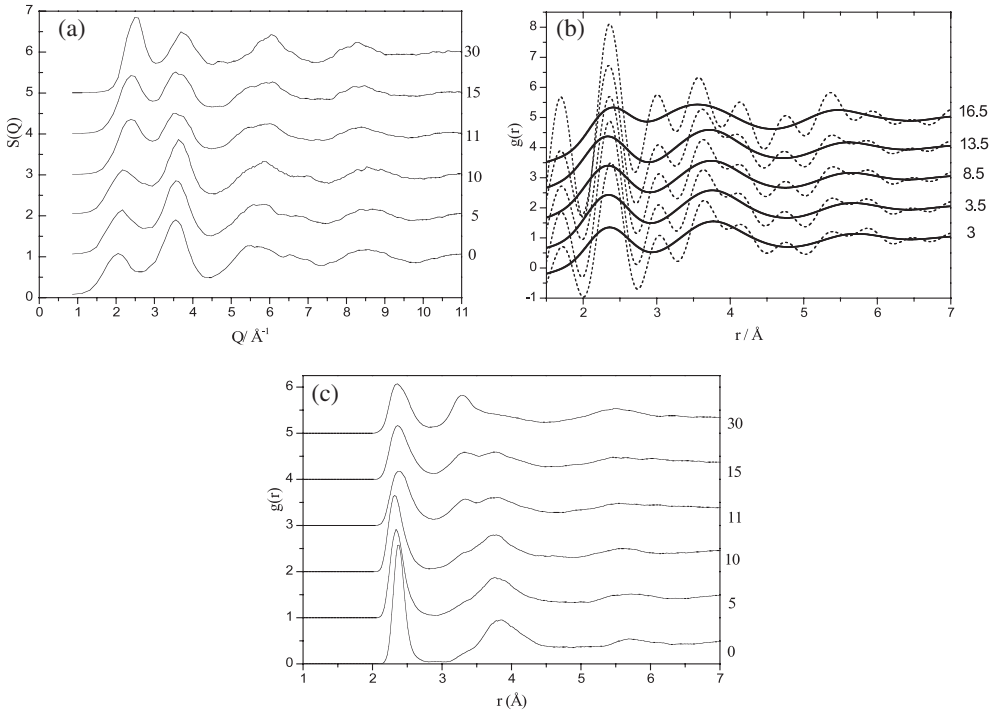

Figure 14. (a) Amorphous scattering structure factors and (d) Si–Si pair distribution functions obtained from MD simulations using a Stillinger–Weber potential function as a function of the pressure (indicated in GPa on the right axis). (b) Si $\cdots$ Si pair distribution functions, $g(r)$, obtained from the x-ray experiments by Fourier transformation of $S(Q)$ amorphous scattering data, as a function of pressure. The dashed and solid lines show the results of Fourier transformation without and with a Blackman windowing function applied to the data, to account for the finite extent of the data in Q space. (c) Pair distribution functions, $g(r)$, obtained from the MD simulations [75].

such microscopic defects [189]. It is in fact possible to obtain analogous configurations using the unmodified SW potential, but only with much slower cooling rates from the liquid state.

The structure of LDA a-Si is that of an essentially ideal tetrahedrally linked network, containing very few over- or under-coordinated defects. The HDA structure can be understood in terms of a large proportion of highly coordinated defects generated within the tetrahedral network [75, 86]. The mean atom coordination number is thus increased to above four by the presence of five-coordinated (or even six-coordinated) atoms that occupy 'defect' sites appearing between the tetrahedra (figure 15). *In situ* high-P studies have also been carried out to investigate the LDA–HDA transformation behaviour of the analogous tetrahedrally coordinated material a-Ge at high P using x-ray scattering and XAS/EXAFS methods, and similar models have been proposed for the amorphous structure at high densities [57, 75, 76, 175, 190].

It was noted above that our analysis of the amorphous x-ray scattering in DAC experiments at high P was hampered by the appearance of Bragg peaks due to metastable crystallization of the β-Sn structured phase of Si [75] (figure 13). The effects of such partial crystallization were not observed in our earlier work using Raman scattering, because the probe beam ($\sim$3–5 μm) in that study was much smaller than the sample area within the DAC (i.e. 120–150 μm) [28] (figure 12). The synchrotron x-ray beam used at ID-15 of the ESRF could only be reduced

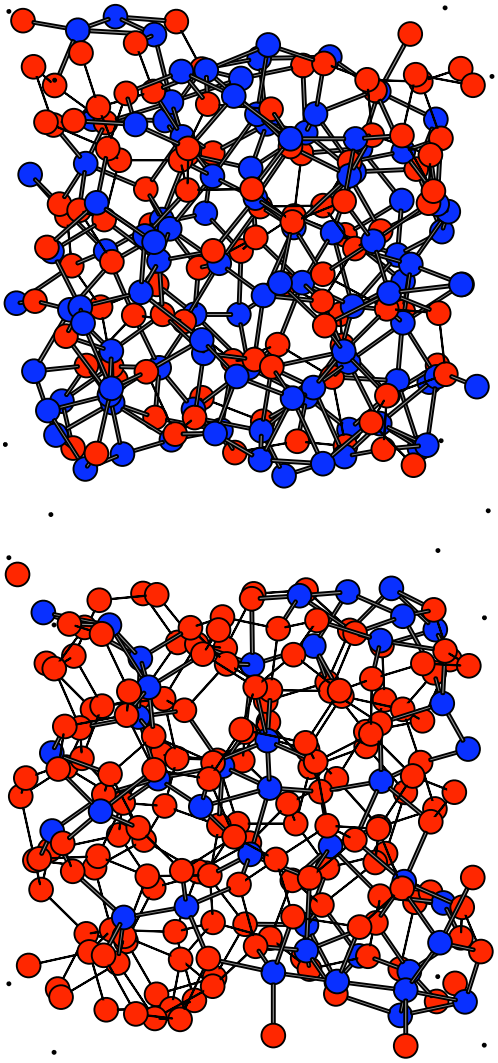

Figure 15. Molecular graphics 'snapshots' of HDA (above) and LDA (below) configurations obtained from low- and high-density S–W MD simulations of Si liquids within the low- and high-density excursions recorded just above the L–L transition point (see figure 17). Four- and five-coordinated Si atoms are shown as red (light) and blue (dark) shaded circles respectively, highlighting the greater number of five-coordinated 'defect' sites in the dense amorphous HDA configuration.

to $\sim$100 μm $\times$ 100 μm, that allowed us to obtain amorphous scattering spectra with no contamination from the gasket material surrounding the sample (figure 13). Essentially the entire sample volume was sampled in the experiment, so that any crystals that nucleated gave a contribution to the scattering signal. We recently conducted new experiments at ID-27 of the ESRF, where the incident x-ray beam could be focused to $\sim$5 μm, i.e. comparable to the probe beam used in laboratory Raman scattering experiments. The synchrotron beam could be scanned relative to the sample, to select those regions that showed no Bragg peaks appearing in the spectrum (figures 13, 16). Preliminary analyses of the results indicate that

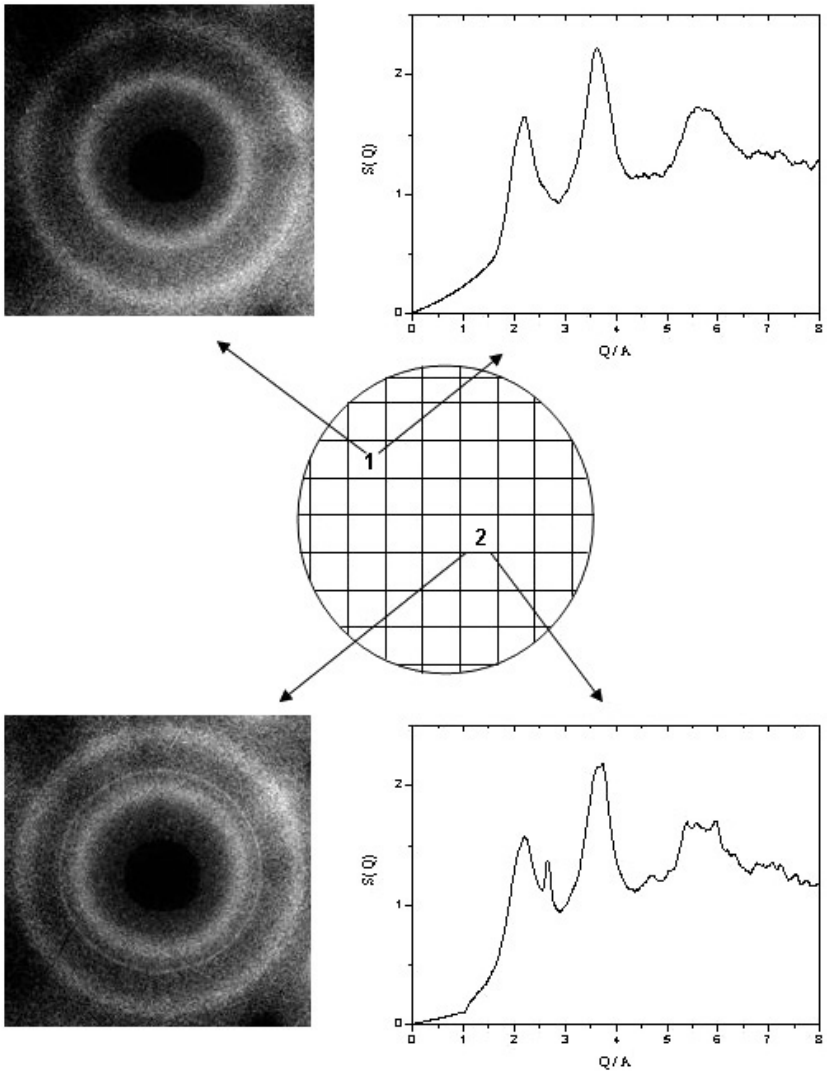

Figure 16. Example of spatially resolved amorphous x-ray diffraction data obtained using the highly focused/collimated beam available at the ESRF, station ID-27, using incident radiation with $\lambda = 0.26472$ Å (46.8 keV). Spectra shown here were obtained from two different regions of the sample within the DAC with a beam size of 3 μm × 5 μm. The pressure in this sample is ∼3 GPa during a decompression run. The top panel taken at the top left within the sample shows only amorphous Laue rings along with the integrated $S(Q)$ for a region of the sample that contained no Bragg diffraction peaks. The lower panel is from another region within the sample that shows the presence of β-Sn structured crystals. Such spatially resolved micro-focus studies of polyamorphism within the DAC and perhaps large-volume devices will become critically important in future studies at high P and under high-P, variable-T conditions using synchrotron x-ray and neutron scattering techniques.

such 'clean' x-ray scattering spectra of a-Si at high P could be obtained throughout its LDA–HDA transition and the back-transformation during recovery to ambient conditions, that agree well with our previous results obtained after subtraction of the Bragg features from the spectra (figure 13) [75].

MD simulations using *ab initio* theoretical methods have also been carried out to investigate density-induced changes in a-Si [86, 88]. These results are now beginning to raise new questions about the nature of L–L transitions in amorphous semiconductor systems, and the polyamorphism phenomenon in general [75]. Morishita reported an abrupt volume decrease on compressing a-Si at $P \sim 12$ GPa, with a ΔV that was analogous to that obtained using the SW potential [75, 86]. As discussed previously, the structural change across the LDA–HDA transition is interpreted as formation of mainly five-coordinated 'defects' within the tetrahedrally coordinated amorphous network. However, the volume change found by Duranduru and Drabold was significantly larger [88]. The volume of the 'very high-density amorphous' (VHDA) form of a-Si lies close to that found in high-pressure crystalline phases, such as the β-Sn (Si-II) and simple hexagonal (Si-V) structured polymorphs, which contain six- and eight-coordinated atoms, respectively [11, 75]. We might expect the local coordination environments associated with the VHDA polyamorph to resemble the local (high-) coordination environments displayed by these high-pressure crystals. Such VHDA forms have already been proposed for both amorphous silicon and germanium based on the application of high pressure to the respective liquids [191]. Funamori and Tsuji noted a change in the structure of liquid silicon between 8 and 14 GPa to give a system whose local coordination environment was suggested to be similar to that of the simple hexagonal crystal [77]. Similarly, Koga *et al* demonstrated how application of high pressure to liquid Ge resulted in an increase in the average coordination number to ∼7 [192]. The larger volume change and significantly higher average coordination number observed in these studies could be indicative of a 'very high-density amorphous' (VHDA) state, analogous to amorphous H_2O [39, 71, 111, 191].

There is now substantial evidence from both simulations and experimental studies that the LDA/HDA transformation in amorphous or liquid Si and Ge as well as H_2O maps on to a first-order thermodynamic phase transition occurring within the supercooled liquid state [7, 9, 28, 31, 38, 55, 96, 108]. However, it is not clear that the same would hold true for the proposed HDA/VHDA transformations. One possibility is that the transition from an HDA-like to a VHDA-like configuration could be continuous and associated with a gradual increase in the number of filled 'defect' sites within the same amorphous structure as P is increased. An alternative possibility is that there does exist a true HDA/VHDA phase transition, associated with a critical point and phase boundary within the system. A natural extension of this argument is that there might exist various distinct liquid or polyamorphic phases as a function of the density, separated from each other by a series of boundaries in P–T space (figure 1). Our experimental studies to date have not allowed us to test the HDA–VHDA hypothesis for a-Si during pressurization at $T = 300$ K. During all of our studies carried out using Raman scattering in the laboratory or at the highly focused x-ray beam at ESRF ID-27, our samples always crystallized spontaneously at $P > 18$ GPa. It will be a major challenge for future *in situ* scattering experiments on amorphous semiconductors to study the structure of such highly compressed amorphous semiconductors, and also to unravel the various metastable crystal–amorphous relationships occurring in this highly metastable regime.

Carrying out MD simulation studies also allowed us to make essential links between the polyamorphism observed in the solid amorphous state at $T = 300$ K, and the density-, entropy-driven L–L transition behaviour predicted to occur at high T, within the supercooled liquid. This transition is generally inaccessible to experimental studies, due to the very rapid crystallization kinetics that occur within the highly fluid semiconductor systems. The result is that experimental observations of the expected polyamorphism for solid a-Si and a-Ge at room T are achieved in a non-ergodic regime, well below the glass transformation range. Generally, it is expected that each of the HDL and LDL liquids will encounter separate glass transformations as the T is lowered, below which they become the non-ergodic HDA or LDA amorphous solids,

that no longer represent true phases within internal thermodynamic equilibrium. However, P-induced transformations between these polyamorphs can be considered to map on to the LDL–HDL polyamorphic liquid–liquid phase transitions, if we assume some similarity between the configurational energy landscapes of the LDA–LDL and HDA–HDL polymorphs. Fast-timescale experiments have predicted that a glass transition temperature should occur for the LDL phase of a-/l-Si at $T_g^L \sim 800$–950 K, extrapolated to 'normal' cooling rates [193, 194]. The corresponding HDL glass transition temperature is still not completely characterized, although a value of $T_g^H \sim 1027$ K is suggested from MD simulations and thermodynamic considerations [55, 75, 96].

We performed simulations for molten Si along isotherms extending down to 1100 K in the supercooled liquid state, to just above the critical point predicted for the HDL–LDL transition by Sastry and Angell [96]. When the system was equilibrated at high T, the volume showed only the small fluctuations about the mean liquid value as expected from thermal (vibrational) fluctuations and diffusion processes. However, as the T_c was approached from above, we observed the appearance of large and random density fluctuations that appeared to oscillate about two mean values that corresponded to low- and high-density states within the single-phase liquid (figure 17). This behaviour is analogous to that already described above for the polyamorphic Y_2O_3–Al_2O_3 liquids just above the liquid–liquid phase transition temperature. The frequency and amplitude of these random density fluctuations are accentuated as T is reduced to approach the L–L transition point.

The observation of this volume fluctuation behaviour is consistent with a 'two-basin' description of the configurational energy hypersurface for the liquid. The thermal energy within the system is larger than or comparable with the energy barriers separating the basins, but these are sufficiently high that the sampling is not fully random; i.e., the system spends various periods of time oscillating about the volume extremes that are expected to become the HDL and LDL liquid states below the L–L phase transition (figure 17(a)). Here we show molecular graphics 'snapshots' of the configurations present for the low- and high-density extrema of the equilibrated liquid, from an MD simulation carried out just above T_c, in the range for which such dynamic nanoscale fluctuations are present (figure 17(b)). The five- and four-coordinated sites present in each have been coloured to aid the structural interpretation of these results. There is obvious clustering of the higher-coordinated sites, that we believe is associated with the regions of low- and high-density states recorded at this T and P. It is expected that such fluctuations should appear in the SAXS or SANS spectra of supercooled Si (and Ge) liquids, on close approach to the predicted L–L transition point.

In the case of liquid Ge, Filipponi, Di Cicco *et al* have carried out XAS and EXAFS studies of deeply undercooled liquid Ge using levitation techniques [84]. As for liquid Si, the high-T Ge liquid is metallic and it contains atoms with an average coordination higher than the tetrahedrally coordinated crystalline semiconductor or the solid amorphous form. This structure is maintained as the liquid is supercooled, until the system spontaneously and rapidly crystallizes into the diamond-structured phase at a T close to that predicted for the onset of the L–L phase transition [1]. Analogous behaviour is recorded for supercooled liquid Si studied by x-ray diffraction [80, 153]. We suggest that the large LDL–HDL fluctuations developed in the metastable supercooled liquid just above the L–L transition point allow the system to sample the low-density configurations, that include the deep potential well associated with the stable diamond-structured crystal. This interpretation would help explain the enormous difficulties associated with quenching bulk Si or Ge glasses from their respective melts. However, the example of polyamorphic Y_2O_3–Al_2O_3 liquids shows that it is in fact possible to kinetically arrest the L–L phase transition process and recover metastably coexisting LDA and HDA glasses, in systems for which the energy barriers within each configurational basin

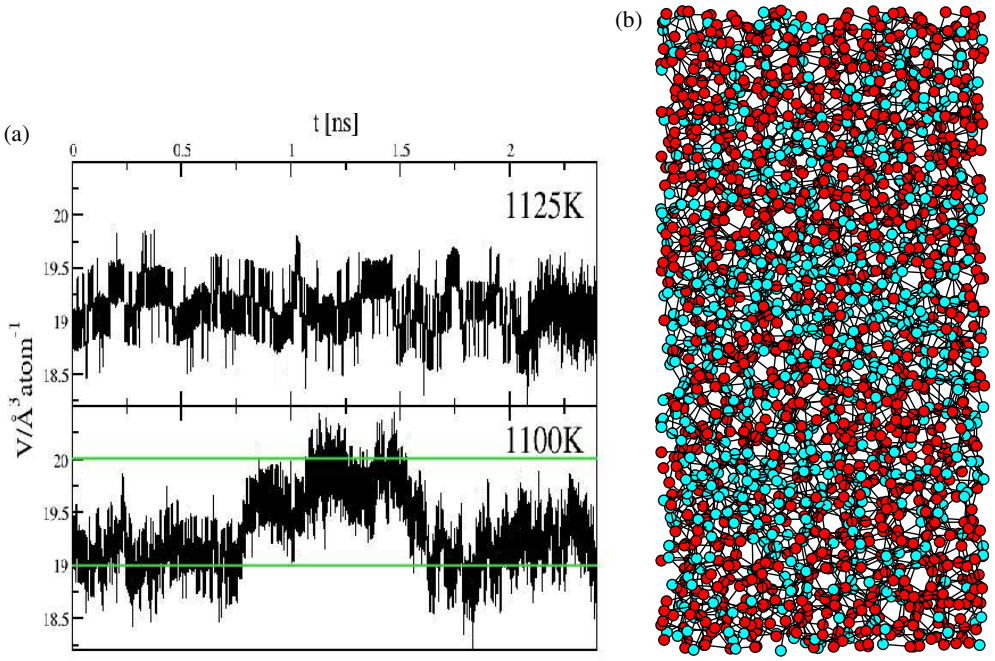

Figure 17. MD-determined density fluctuations in liquid Si on approach to the predicted L–L phase transition. (a) The system volume (V) plotted for l-Si as a function of the simulation time after nominal equilibration at $T = 1075$ K and $P \sim 1$ atm, i.e. just above the L–L transition point, shows significant random fluctuations in the cell volume. (b) A $U(V)$ map created for a single-phase liquid under P–T conditions just above the predicted L–L transition shows a 'two-basin' structure, supporting the concept of a two-domain liquid system containing distinct high- and low-density families of configurational states, that are being sampled semi-randomly at a T just exceeding the thermal energy provided to the system at that point. (b) Molecular graphics 'snapshot' of a configuration of Si taken from a molecular dynamics simulation at 1075 K and zero pressure, indicating the likely appearance of nanoscale low- and high-density domains within the single-liquid phase structure at temperatures just above the macroscopic T_c or T_{L-L} transitions that might be detected by future small-angle x-ray or neutron scattering studies. The atoms are coloured by their nearest-neighbour coordination number (four coordinated—red, five coordinated—blue). Regions high in five-coordinated sites (HDL-like) and in four-coordinated sites (LDL-like) are clearly evident.

are sufficiently high, or where there is little possibility of achieving a crystalline structure. Investigating the onset of such nanoscale fluctuations that exist just above the T_c or T_{LL} for density-driven L–L phase transitions could also become technologically important, as a means of designing and creating nanocomposite glass–ceramic materials, with enhancement of their mechanical strength and incorporation of other desirable physical properties.

4. Conclusions and future challenges for experimental and theoretical studies of polyamorphism and liquid–liquid phase transitions

The likelihood that first-order density- or entropy-driven phase transitions occur in the liquid state at constant chemical composition, analogous to polymorphic phase changes that appear among crystalline solids as a function of P and T, is now well supported by experimental and theoretical studies. Because it is likely that most density-, entropy-driven L–L phase transitions occur below the liquidus, their experimental study is faced with two major challenges. First,

they must be explored and established experimentally by structural studies and determination of the thermodynamic properties *in situ*, under combined high-P, variable-T conditions, including cryogenic low temperatures, and even extending into the negative-pressure (tensile) regime for some systems. Next, the fact that much L–L transition behaviour occurs in the supercooled liquid regime means that it competes with stable versus metastable crystallization phenomena, that can overwhelm the results and obscure their interpretation. It is essential to study and establish L–L phase transition phenomena, because they constitute an important completion of the thermodynamic rules established for condensed matter, extended to the liquid state. It is already well known that liquid unmixing occurs in response to the chemical potential variable (μ (X)); density-, entropy-driven transitions can appear at constant chemical composition even for elemental substances, as a function of the P and T. We can even presume that, just like crystalline polymorphs, a sequence of L–L transitions might appear as a function of increasing density, with the lowest-pressure transition occurring between an LDL liquid and the gas phase (figure 1). The phenomenology is not restricted to any particular type of chemical bonding or interatomic packing; evidence for the occurrence of L–L transitions or their polyamorphic equivalent in the non-ergodic solid amorphous state occurs for all classes of elements and compounds, with all types of bonding interaction. In fact, the phenomenology is readily extended to and appears to apply to nanoscale systems such as polymer bead assemblies, interacting via hard or soft potential energy functions.

Liquid–liquid transitions at constant chemical composition are already well described among the liquid crystal community, in which the metastable liquid phases are distinguished by ordering patterns among the polymer units. Here, the dominant interactions are the covalent bonding forces maintaining the polymer chains; weaker van der Waals interactions between the chains or ionic ordering forces cause the appearance of liquid crystal phases with well defined thermodynamic properties and phase transitions between them. However, these represent a small family of compounds with a special case of interactions between the components: density-, entropy-driven L–L phase transitions are likely occur quite generally, among all class of liquids with various bonding and interaction types. The theoretical challenges consist in addressing density- and entropy-driven transitions that occur among the wide range of liquid systems, in a highly supercooled regime, using simulation sizes that are large enough to capture the macroscopic nucleation and growth of a second liquid phase, and to study the behaviour on approach to the homogeneous stability limits within the low- and high-density phases. As new calculations with 'million-atom' simulations begin to appear, we should begin to properly observe the appearance of nanoscale fluctuation domains within the liquids above the critical point, and evaluate their contributions to the x-ray and neutron scattering data.

Acknowledgments

Our work on polyamorphism has been supported by the US-NSF, EPSRC, UCL, RI and UW Aberystwyth, as well as the Wolfson Foundation-Royal Society through a Research Merit Award to PFM. Neutron experiments were performed at the Intense Pulsed Neutron Source (Argonne National Laboratory, USA) and ISIS (RAL, UK). High-energy x-ray diffraction studies were performed at the APS (US DOE), SRS (station 6.2) and ESRF. PFM is an EPSRC Senior Research Fellow (2007-1012).

References

[1] Ponyatovsky E G and Barkalov O I 1992 *Mater. Sci. Rep.* **8** 147
[2] Debenedetti P G 1997 *Metastable Liquids* (Princeton, NJ: Princeton University Press)

[3] Poole P H, Grande T, Angell C A and McMillan P F 1997 *Science* **275** 322
[4] Angell C A 1995 *Science* **267** 1924
[5] Angell C A, Ngai K L, McKenna G B, McMillan P F and Martin S W 2000 *J. Appl. Phys.* **88** 3113
[6] Brazhkin V V, Buldyrev S V, Ryzhov V N and Stanley H E (ed) 2002 *New Kinds of Phase Transitions: Transformations in Disordered Substances* (Dordrecht: Kluwer)
[7] McMillan P F 2004 *J. Mater. Chem.* **14** 1506
[8] Tanaka H 2000 *Phys. Rev.* E **62** 6968
[9] Mishima O and Stanley H E 1998 *Nature* **396** 329
[10] Bridgman P W 1949 *The Physics of High Pressure* (London: Bell)
[11] Liu L-G and Bassett W A 1986 *Elements, Oxides, and Silicates. High-Pressure Phases with Implications for the Earth's Interior* (Oxford: Clarendon)
[12] Boehler R 1996 *Phil. Trans. R. Soc.* A **354** 1265
[13] Nguyen J H and Homes N C 2004 *Nature* **427** 339
[14] Errandonea D, Somayazulu M, Hausermann D and Mao H-K 2003 *J. Phys.: Condens. Matter* **15** 7635
[15] Alfè D, Vocadlo L, Price G D and Gillan M J 2004 *J. Phys.: Condens. Matter* **16** S973
[16] Brygoo S, Henry E, Loubeyre P, Eggert J, Koenig M, Loupias B, Benuzzi-Mounaix A and Rabec Le Gloahec M 2007 *Nat. Mater.* **6** 274
[17] Rapoport E 1967 *J. Chem. Phys.* **46** 2891
[18] Bundy F P, Bassett W A, Weathers M S, Hemley R J, Mao H-K and Goncharov A F 1996 *Carbon* **34** 141
[19] Ferraz A and March N H 1979 *Phys. Chem. Liquids* **8** 289
[20] van Thiel M and Ree F H 1993 *Phys. Rev.* B **48** 3591
[21] Moore W J 1972 *Physical Chemistry* (New York: Prentice Hall)
[22] Eisenberg D and Kauzmann W 1969 *The Structure and Properties of Water* (London: Oxford University Press)
[23] Stanley H E, Buldyrev S V, Franzese G, Giovambattista N and Starr F W 2005 *Phil. Trans. R. Soc.* A **363** 509
[24] Wilson M and McMillan P F 2003 *Phys. Rev. Lett.* **90** 135703
[25] Guggenheim E A 1949 *Thermodynamics. An Advanced Treatment for Chemists and Physicists* (Amsterdam: North-Holland)
[26] Aptekar L I 1979 *Sov. Phys. Dokl.* **24** 993
[27] Deb S K, Wilding M C, Somyazulu M and McMillan P F 2001 *Nature* **414** 528
[28] McMillan P F, Wilson M, Daisenberger D and Machon D 2005 *Nat. Mater.* **4** 680
[29] Rapoport E 1967 *J. Chem. Phys.* **46** 2891
[30] Moynihan C T and Angell C A 2000 *J. Non-Cryst. Solids* **274** 131
[31] Angell C A, Bressel R D, Hemmatti M, Sare E J and Tucker J C 2000 *Phys. Chem. Chem. Phys.* **2** 1559
[32] Kurita R and Tanaka H 2005 *J. Phys.: Condens. Matter* **17** L293
[33] Tanaka H 2000 *Europhys. Lett.* **50** 340
[34] Aasland S and McMillan P F 1994 *Nature* **369** 633
[35] Mishima O, Calvert L D and Whalley E 1985 *Nature* **314** 76
[36] Poole P H, Sciortino F, Essmann U and Stanley H E 1992 *Nature* **360** 324
[37] Sciortino F, Poole P H, Essmann U and Stanley H E 1997 *Phys. Rev.* E **55** 727
[38] Angell C A 2004 *Annu. Rev. Phys. Chem.* **55** 559
[39] Loerting T and Giovambattista N 2006 *J. Phys.: Condens. Matter* **18** R919
[40] Katayama Y, Inamura Y, Mizutani T, Yamakata M, Utsumi W and Shimomura O 2004 *Science* **306** 848
[41] Katayama Y, Mizutani T, Utsumi W, Shimomura O, Yamakata M and Funakohi K-I 2000 *Nature* **403** 170
[42] Monaco G, Falconi S, Crichton W A and Mezouar M 2003 *Phys. Rev. Lett.* **90** 255701
[43] McMillan P F 2000 *Nature* **403** 151
[44] Brazhkin V V, Popova S V and Voloshin R N 1997 *High Pressure Res.* **15** 267
[45] Brazhkin V V, Popova S V and Voloshin R N 1999 *Physica* B **265** 64
[46] Ha A, Cohen I, Zhao X, Mlee M and Kivelson D 1996 *J. Phys. Chem.* **100** 022
[47] Tanaka H, Kurita R and Mataki H 2004 *Phys. Rev. Lett.* **92** 025701
[48] Demirjian B G, Dosseh G, Chauty A, Ferrer M-L, Morineau D, Lawrence C, Takeda K and Kivelson D 2001 *J. Phys. Chem.* **105** 2107
[49] Cohen I, Ha A, Zhao X, Lee M, Fischer T, Strouse M J and Kivelson D 1996 *J. Phys. Chem.* **100** 8518
[50] Kurita R and Tanaka H 2004 *Science* **306** 845
[51] Olsen N B, Christensen T and Dyre J C 2001 *Phys. Rev. Lett.* **86** 1271
[52] Donovan E P, Spaepen F, Turnbull D, Poate J M and Jacobson D D 1983 *Appl. Phys. Lett.* **42** 698
[53] Wilding M C, McMillan P F and Navrotsky A 2002 *J. Phys. Chem. Glasses* **43** 306
[54] Wilding M C, McMillan P F and Navrotsky A 2002 *Physica* A **314** 379
[55] Angell C A, Borick S and Grabow M 1996 *J. Non-Cryst. Solids* **205–207** 463
[56] Majérus O, Cormier L, Itié J-P and Calas G 2005 *Phys. Scr.* T **115** 525

[57] Di Cicco A, Principi E, Minicucci M, De panfilis S, Filipponi A, Decremps F, Datchi F, Itié J-P, Munsch P and Polian A 2004 *High Pressure Res.* **24** 93
[58] Itié J-P, Polian A, Calas G, Petiau J, Fontaine A and Tolentino H 1989 *Phys. Rev. Lett.* **63** 398
[59] Filipponi A 2001 *J. Phys.: Condens. Matter* **13** R23
[60] Greaves G N 1985 *J. Non-Cryst. Solids* **71** 203
[61] Greaves G N and Sen S 2007 *Adv. Phys.* **56** 1
[62] Fischer H E, Barnes A C and Salmon P S 2006 *Rep. Prog. Phys.* **69** 233
[63] Wilding M C and Benmore C 2006 *Rev. Mineral. Geochem.* **63** 275
[64] McMillan P F, Wilson M and Wilding M C 2003 *J. Phys.: Condens. Matter* **15** 6105
[65] Guthrie M, Tulk C A, Benmore C J, Xu J, Yarger J L, Klug D D, Tse J S, Mao H-K and Hemley R J 2004 *Phys. Rev. Lett.* **93** 115502
[66] Yamanaka T, Sugiyama K and Ogata K 1992 *J. Appl. Crystallogr.* **25** 11
[67] Ohtaka O, Yoshiasa A, Fukui H, Murai K-I, Okube M, Katayama Y, Utsumi W and Nishihata Y 2001 *J. Synchrotron Res.* **8** 791
[68] Meade C, Hemley R J and Mao H-K 1992 *Phys. Rev. Lett.* **69** 1387
[69] Koza M M, Hansen T, May R P and Schober H 2006 *J. Non-Cryst. Solids* **352** 4988
[70] Koza M M, May R P and Schober H 2006 *J. Appl. Crystallogr.* **40** S517
[71] Nelmes R J, Loveday J S, Strässle T, Bull C L, Guthrie M, Hamel G and Klotz S 2006 *Nature Phys.* **2** 414
[72] Tulk C A, Benmore C, Urquidi J, Klug D D, Neuefeind J, Tomberli B and Egelstaff P A 2002 *Science* **297** 1320
[73] Crichton W A, Mezouar M, Grande T, Stolen S and Grzechnik A 2001 *Nature* **414** 622
[74] Raty J Y, Gaspard J P, Le bihan T, Mezouar M and Bionducci M 1999 *J. Phys.: Condens. Matter* **11** 10243
[75] Daisenberger D, McMillan P F, Wilson M, Machon D, Quesada-cabrera R and Wilding M C 2007 *Phys. Rev.* B **75** 224118
[76] Tanaka K 1991 *Phys. Rev.* B **43** 4302
[77] Funamori N and Tsuji K 2002 *Phys. Rev. Lett.* **88** 255508/1
[78] Shen G, Prakapenka V B, Rivers M L and Sutton S R 2003 *Rev. Sci. Instrum.* **74** 3021
[79] Eggert J H, Weck G, Loubeyre P and Mezouar M 2002 *Phys. Rev.* B **65** 174105
[80] Ansell A, Krishnan S, Felten J J and Price D L 1998 *J. Phys.: Condens. Matter* **10** L73
[81] Kim T H, Lee G W, Sieve B, Gangopadhya A K, Hyers R W, Rathz T J, Rogers J R, Robinson D S, Klton K F and Goldman A I 2005 *Phys. Rev. Lett.* **95** 085501/1
[82] Weber J K R, Felten J J, Cho B and Nordine P C 1998 *Nature* **393** 769
[83] Wilding M C and McMillan P F 2002 *New Kinds of Phase Transitions: Transformations in Disordered Substances* ed V V Brazhkin, S V Buldyrev, V N Ryzhov and H E Stanley (Dordrecht: Kluwer) pp 57–73
[84] Filipponi A and Di Cicco A 1995 *Phys. Rev.* B **51** 12322
[85] Wilding M C, Wilson M and McMillan P F 2006 *Chem. Soc. Rev.* **35** 964
[86] Morishita T 2004 *Phys. Rev. Lett.* **93** 055503/1
[87] Ashwin S S, Waghmare U V and Sastry S 2004 *Phys. Rev. Lett.* **92** 175701
[88] Duranduru M and Drabold D A 2001 *Phys. Rev.* B **64** 014101/1
[89] Tse J S, Klug D D and Le Page Y 1992 *Phys. Rev.* B **46** 5933
[90] Duranduru M and Drabold D A 2002 *Phys. Rev.* B **65** 104208/1
[91] Wilson M and McMillan P F 2004 *Phys. Rev.* B **69** 54206
[92] Wilding M C, Wilson M and McMillan P F 2005 *Phil. Trans. R. Soc.* A **363** 598
[93] Poole P H, Hemmati M and Angell C A 1997 *Phys. Rev. Lett.* **79** 2281
[94] Saika-Voivod L, Sciortino F and Poole P H 2001 *Phys. Rev.* E **63** 011202
[95] Saika-Voivod L, Sciortino F and Poole P H 2004 *Phil. Mag.* **84** 1437
[96] Sastry S and Angell C A 2003 *Nat. Mater.* **2** 739
[97] Saika-Voivod L, Poole P H and Sciortino F 2001 *Nature* **412** 514
[98] Huang L, Duffrène L and Kieffer J 2004 *J. Non-Cryst. Solids* **349** 1
[99] Roberts C J and Debenedetti P G 1996 *J. Chem. Phys.* **105** 658
[100] Tse J S E A 2005 *Phys. Rev.* B **71** 214107
[101] Angell C A, Wang L-M, Mossa S, Yue Y and Copley J R D 2004 in *Slow Dynamics in Complex Systems: 3rd Int. Conf.* ed M Tokuyama and I Oppenheim (New York: American Institute of Physics) pp 473–82
[102] Morishita T 2005 *Phys. Rev.* E **72** 021201/1
[103] Kurita R and Tanaka H 2007 *J. Chem. Phys.* **126** 204505
[104] Mishima O, Calvert L D and Whalley E 1984 *Nature* **310** 393
[105] Bowron D T, Finney J L, Hallbrucker A, Kohl I, Loerting T, Mayer E and Soper A K 2006 *J. Chem. Phys.* **125** 194502
[106] Whalley E, Klug D D and Handa Y P 1989 *Nature* **342** 782
[107] Mishima O 1994 *J. Chem. Phys.* **100** 5910

[108] Mishima O and Suzuki Y 2002 *Nature* **419** 599
[109] Koza M M, Schober H, Fischer H E, Hansen T and Fujara F 2003 *J. Phys.: Condens. Matter* **15** 321
[110] Giovambattista N, Stanley H E and Sciortino F 2005 *Phys. Rev. Lett.* **94** 107803/1
[111] Loerting T, Salzmann C, Kohl I, Mayer E and Hallbrucker A 2001 *Phys. Chem. Chem. Phys.* **3** 5355
[112] Finney J L, Bowron D T, Soper A K, Loerting T, Mayer E and Hallbrucker A 2002 *Phys. Rev. Lett.* **89** 205503
[113] Brazhkin V V, Voloshin R N, Popova S V and Umnov A G 1992 *J. Phys.: Condens. Matter* **4** 1419
[114] Greenwood N N and Earnshaw A 1984 *Chemistry of the Elements* (Oxford: Pergamon)
[115] Cotton F A and Wilkinson G W 1972 *Advanced Inorganic Chemistry* (New York: Wiley)
[116] Zallen R 1983 *The Physics of Amorphous Solids* (New York: Wiley)
[117] Wilding M C and McMillan P F 2001 *J. Non-Cryst. Solids* **293** 357
[118] Wilding M C, Benmore C and McMillan P F 2002 *J. Non-Cryst. Solids* **297** 143
[119] Wilding M C and McMillan P F 2002 *New Kinds of Phase Transitions: Transformation in Disordered Substances* ed V V Brazhkin, S V Buldyrev, V N Ryzhov and H E Stanley (Dordrecht: Kluwer) p 57
[120] Wilding M C and McMillan P F 2002 *Phys. Chem. Glass.* C **43** 451
[121] Wolf G H, Wang S, Herbst C A, Durben D J, Oliver W F, Kang Z C and Halvorson K 1992 *High-Pressure Research: Application to Earth and Planetary Sciences* ed Y Syono and M H Manghnani (Washington, DC: American Geophysical Union) p 503
[122] Yarger J L, Angell C A, Borick S S and Wolf G H 1997 *Supercooled Liquids. Advances and Novel Applications* ed J T Fourkas, D Kivelson, U Mohanty and K A Nelson (Washington, DC: American Chemical Society) p 214
[123] Hemley R J, Mao H K, Bell P M and Mysen B O 1986 *Phys. Rev. Lett.* **57** 747
[124] McMillan P, Piriou B and Couty R 1984 *J. Chem. Phys.* **81** 4234
[125] Bridgman P W and Simon I 1953 *J. Appl. Phys.* **24** 405
[126] Sakka S and Mackenzie J D 1969 *J. Non-Cryst. Solids* **1** 107
[127] Mackenzie J D 1963 *J. Am. Ceram. Soc.* **46** 470
[128] Mackenzie J D 1963 *J. Am. Ceram. Soc.* **46** 461
[129] Barker L M and Hollenback R E 1970 *J. Appl. Phys.* **41** 4208
[130] Bruckner R 1970 *J. Non-Cryst. Solids* **5** 123
[131] Wolf G H and McMillan P F 1995 *Structure, Dynamics and Properties of Silicate Melts* ed J F Stebbins, P F McMillan and D B Dingwell (Washington, DC: Mineralogical Society of America) p 505
[132] Susman S, Volin K J, Price D L, Grimsditch M, Rino J P, Kalia R K, Vashishta P, Gwanmesia G, Wang Y and Liebermann R C 1991 *Phys. Rev.* B **43** 1194
[133] Smith K H, Shero E, Chizmeshya A and Wolf G H 1995 *J. Chem. Phys.* **102** 6851
[134] Cohen H M and Roy R 1965 *Phys. Chem. Glasses* **6** 149
[135] Grimsditch M 1984 *Phys. Rev. Lett.* **52** 2379
[136] Grimsditch M 1986 *Phys. Rev.* B **34** 4372
[137] Wackerle J 1962 *J. Appl. Phys.* **33** 922
[138] Schmitt D R and Ahrens T J 1989 *J. Geophys. Res.* **94** 5851
[139] Marsh S P 1980 *LASL Shock Hugoniot Data* (Berkeley, CA: University of California Press) p 321
[140] Hemley R J, Jephcoat A P, Mao H K, Ming L C and Manghnani M 1988 *Nature* **334** 52
[141] Williams Q and Jeanloz R 1988 *Science* **239** 902
[142] Williams Q, Hemley R J, Kruger M B and Jeanloz R 1993 *J. Geophys. Res.* **98** 22157
[143] Hemley R J, Prewitt C T and Kingma K J 1994 *Rev. Mineral.* ed P Heaney, G V Gibbs and C T Prewitt (Washington, DC: Mineralogical Society of America) p 41
[144] Charles R J 1967 *J. Am. Ceram. Soc.* **50** 631
[145] McMillan P and Piriou B 1983 *J. Non-Cryst. Solids* **55** 221
[146] Domene C, Fowler P W, Wilson M and Madden P A 2002 *Mol. Phys.* **100** 3847
[147] Madden P A and Wilson M 1996 *Chem. Soc. Rev.* **25** 339
[148] Jahn S, Madden P A and Wilson M 2006 *Phys. Rev.* B **74** 024112
[149] Wilding M C, Greaves G N, Hennet L, Fearn S and Weber J K R 2007 in preparation
[150] Krishnan S, Felten J J, Rix J E, Weber J K R, Nordine P C, Ansell S, Beno M A and Price D L 1997 *Rev. Sci. Instrum.* **68** 3512
[151] Wilding M C, Greaves G N, Benmore C and Weber J K R 2006 *Proc. SRMS-5 Conf. (Chicago)* p 299
[152] Ansell A, Krishnan S, Felten J J and Price D L 1999 *J. Phys.: Condens. Matter* **11** 8167
[153] Jakse N, Hennet L, Price D L, Krishnan S, Key T, Artacho E, Glorieux B, Pasturel A and Saboungi M-L 2003 *Appl. Phys. Lett.* **83** 4734
[154] Krishnan S, Hennet L, Jahn S, Key T A, Madden P A, Saboungi M-L and Price D L 2005 *Chem. Mater.* **17** 2662
[155] Hennet L, Thiaudière D, Landron C, Melin P, Price D L, Bérar J-F and Saboungi M-L 2003 *Appl. Phys. Lett.* **83** 3305

[156] Hennet L, Pozdnyakova I, Greaves G N, Krishnan S, Wilding M, Frean S, Majeus O, Martin C and Price D L 2006 *Proc. SRMS-5 Conf. (Chicago)* p 115
[157] Landron C, Hennet L, Thiaudière D, Price D L and Greaves G N 2003 *Nucl. Instrum. Methods* B **199** 481
[158] Landron C, Hennet L, Coutures J-P, Gailhanou M, Gramond M and Bérar J-F 1998 *Europhys. Lett.* **44** 429
[159] Landron C, Hennet L, Coutures J-P, Jenkins T, Aletru C, Greaves G N, Soper A K and Derbyshire G 2000 *Rev. Sci. Instrum.* **71** 1745
[160] Landron C, Soper A K, Jenkins T, Greaves G N, Hennet L and Coutures J-P 2001 *J. Non-Cryst. Solids* **293** 453
[161] Ansell S, Krishnan S, Weber J K R, Felton J J, Nordine P C, Beno M A, Price D L and Saboungi M-L 1997 *Phys. Rev. Lett.* **78** 464
[162] Landron C, Hennet L, Jenkins T, Greaves G N, Coutures J-P and Soper A K 2001 *Phys. Rev. Lett.* **86** 4839
[163] Sinn H, Glorieux B, Hennet L, Atlas A, Hu M, Alp E E, Bermejo F J, Price D L and Saboungi M-L 2003 *Science* **299** 2047
[164] Poe B T, McMillan P F, Coté B, Massiot D and Coutures J-P 1994 *J. Am. Ceram. Soc.* **77** 1832
[165] Poe B T, McMillan P F, Coté B, Massiot D and Coutures J-P 1993 *Science* **259** 786
[166] Boucher S, Piwowarczyk J, Marzke R F, Takulapalli B, Wolf G H, McMillan P F and Petuskey W T 2005 *J. Eur. Ceram. Soc.* **25** 1333
[167] Coutures J-P, Massiot D, Bessada C, Echegut P, Rifflet J C and Taulelle F 1990 *C. R. Acad. Sci. Paris* **310** 1041–5
[168] Weber J K R, Hampton D S, Merkley D R, Rey C A, Zatarski M M and Nordine P C 1994 *Rev. Sci. Instrum.* **65** 456
[169] Weber J K R, Tangeman J A, Key T S and Nordine P C 2003 *J. Thermophys. Heat Transfer* **17** 182
[170] De Neufville J-P and Turnbull D 1971 *Faraday Soc. Discuss.* **327** 180
[171] Baeri P, Campisaro S U, Grimaldi M G and Rimini E 1982 *J. Appl. Phys.* **53** 8730
[172] Thompson M O, Galvin G J, Mayer J W, Peercy P S, Poate J M, Jacobson D C, Cullis A G and Chew N G 1984 *Phys. Rev. Lett.* **52** 2360
[173] Angell C A and Borick S S 1999 *J. Phys.: Condens. Matter* **11** 8163
[174] Beaucage P and Mousseau N 2005 *J. Phys.: Condens. Matter* **17** 2269
[175] Bhat M H, Molinero V, Soignard E, Solomon V C, Sastry S, Yarger J L and Angell C A 2007 *Nature* at press
[176] Sheng H W, Liu H Z, Cheng Y Q, Wen J, Lee P L, Luo W K, Shastri S D and Ma E 2007 *Nat. Mater.* **6** 192
[177] Minomura S 1978 *High Pressure and Low Temperature Physics* (New York: Plenum) p 483
[178] Shimomura O, Minomura S, Sakai N, Asaumi K, Tamura K, Fukushima J and Endo H 1974 *Phil. Mag.* **29** 547
[179] Imai M, Mitamura T, Yaoita K and Tsuji K 1996 *High Pressure Res.* **15** 167
[180] Fortner J and Lannin J S 1989 *Phys. Rev.* B **39** 5527
[181] Kugler S, Molnár G, Petö G, Zsoldos E, Rosta L, Menelle A and Bellisent R 1989 *Phys. Rev.* B **40** 8030
[182] Laaziri K, Kycia S, Roorda S, Chicoine M, Robertson J L, Wang J and Moss S C 1999 *Phys. Rev. Lett.* **82** 3460
[183] Stillinger F H and Weber T A 1985 *Phys. Rev.* B **31** 5262
[184] Nosé S 1984 *J. Chem. Phys.* **81** 511
[185] Nosé S 1984 *Mol. Phys.* **52** 255
[186] Martyna G J, Tobias D J and Klein M L 1992 *J. Chem. Phys.* **101** 4177
[187] Luedtke W D and Landman U 1989 *Phys. Rev.* B **40** 1164
[188] Luedtke W D and Landman U 1988 *Phys. Rev.* B **37** 4656
[189] Custer J S, Thompson M O, Jacobson D C, Poate J M, Roorda S, Sinke W C and Spaepen F 1994 *Appl. Phys. Lett.* **64** 437
[190] Freund J, Ingalis R and Crozier E D 1990 *J. Phys. Chem.* **94** 1087
[191] Benmore C J, Hart R T, Mei Q, Price D L, Yarger J L, Tulk C A and Klug D D 2005 *Phys. Rev.* B **72** 132201
[192] Koga J, Okumura H, Nishio K, Yamaguchi T and Yonezawa F 2002 *Phys. Rev.* B **66** 064211
[193] Hedler A, Klaumünzer S L and Wesch W 2004 *Nat. Mater.* **3** 804
[194] McMillan P F 2004 *Nat. Mater.* **3** 755